J Comput Neurosci
DOI 10.1007/s10827-012-0389-5

A mathematical model for astrocytes mediated LTP at single hippocampal synapses

Shivendra Tewari · Kaushik Majumdar

Received: 28 July 2011 / Revised: 21 February 2012 / Accepted: 22 February 2012

Abstract Many contemporary studies have shown that astrocytes play a significant role in modulating both short and long form of synaptic plasticity. There are very few experimental models which elucidate the role of astrocyte over Long-term Potentiation (LTP). Recently, Perea and Araque (Science 317:1083–1086, 2007) demonstrated a role of astrocytes in induction of LTP at single hippocampal synapses. They suggested a purely pre-synaptic basis for induction of this N-methyl-D-Aspartate (NMDA) Receptor-independent LTP. Also, the mechanisms underlying this pre-synaptic induction were not investigated. Here, in this article, we propose a mathematical model for astrocyte modulated LTP which successfully imitates the experimental findings of Perea and Araque (Science 317:1083–1086, 2007). Our study suggests the role of retrograde messengers, possibly Nitric Oxide (NO), for this pre-synaptically modulated LTP.

Keywords Astrocytes · Calcium · Calcium/calmodulin-dependent protein kinase II · Long-term potentiation · Nitric oxide

1 Introduction

Long-term Potentiation (LTP), a long form of synaptic plasticity, has long been considered an eminent synaptic model for investigating the molecular basis of memory (Bliss and Collingridge 1993; Collingridge et al. 2004). However, there is still debate regarding its functional relevance—for example, is it a model of memory formation or is it the exact mechanism used by brain to store information (Bliss et al. 2004)? LTP can be induced using different protocols of stimulation, like, theta-burst stimulation (TBS) protocol or primed-burst stimulation (PBS) protocol (Bliss and Collingridge 1993). The significance of these protocols is that similar synchronized firing patterns occur inside hippocampus during learning. LTP can be classified depending upon the need for protein transcription and translation for its induction. LTP which does not require protein transcription and translation is termed as early-phase LTP (e-LTP) and lasts for 2–4 h, whereas, LTP which requires protein transcription and translation is termed as late-phase LTP (l-LTP) and lasts for hours, days or even weeks (Malenka and Bear 2004; Aslam et al. 2009). There is vast amount of literature available over LTP for different experimental models (Bliss and Lomo 1973; Bliss and Collingridge 1993; Malenka and Bear 2004; Anwyl 2009; Aslam et al. 2009).

With the advent of new imaging techniques, it became possible to discover the role of a subtype of glial cells widely distributed in Central Nervous System (CNS): astrocyte (Ben Achour et al. 2010). Araque et al. (1999) coined the term "Tripartite Synapse (TpS)" which considers a peri-synaptic astrocyte, in addition to our classical synapse, of a pre-synaptic neuron and post-synaptic neuron. However, due to spatio-temporal limitations of current imaging techniques it is not easy to study LTP at a specific TpS. Consequently, such experimental observations are few, of relatively recent origin (Perea and Araque 2007; Henneberger et al. 2010) and have remained controversial at least to some extent (Agulhon et al. 2010). In such situations mathematical modeling can be a viable alternative to have hitherto unobserved insights.

Perea and Araque (2007) investigated the consequence of astrocyte calcium (Ca^{2+}) elevations at single hippocampal synapses, in particular Schaffer collateral—CA1 pyramidal

Action Editor: Bard Ermentrout

Electronic supplementary material The online version of this article (doi:10.1007/s10827-012-0389-5) contains supplementary material, which is available to authorized users.

S. Tewari · K. Majumdar (✉)
Systems Science and Informatics Unit, Indian Statistical Institute,
8th Mile, Mysore Road,
Bangalore 560059, India
e-mail: kmajumdar@isibang.ac.in

S. Tewari
e-mail: shivendra.tewari@gmail.com

Published online: 28 March 2012

cell (SC—CA1) synapse. They loaded astrocytes with Ca^{2+}—cage o-nitrophenyl-EGTA (NP-EGTA) stimulated selectively using ultraviolet (UV)—flash photolysis, while simultaneously stimulating SC using minimal stimulation protocol which activates single or few synapses (Perea and Araque 2007). They reported a transient enhancement of probability of neurotransmitter release (Pr), when an astrocyte was stimulated (but not without), accompanied by a transient increase in synaptic efficacy (given as a measure of mean Excitatory Post-Synaptic Current (EPSC) amplitudes, including successes and failures). Further, when they paired astrocyte stimulation with mild depolarization (to -30 mV) of post-synaptic neuron, found persistent increase in Pr, with synaptic efficacy also following likewise, signifying astrocyte modulated LTP.

The LTP observed in their experiments can be classified as e-LTP which has a pre-synaptic locus of induction, because they observed persistent increase in synaptic efficacy along with no-change in synaptic potency (given as a measure of mean EPSC amplitudes of successes). Also, using antagonists, D-2-amino-5-phosphonopentanoic acid (D-AP5), of NMDARs and antagonists, MPEP+LY367385, of group I metabotropic glutamate receptors (mGluRs) they confirmed that the LTP observed was NMDAR-independent with pre-synaptic locus of induction which is more challenging to our vision of classical LTP in CA1 region (Perea and Araque 2007). Here, in this article we present, a very comprehensive computational model of TpS which provides a mathematical framework for astrocyte modulated NMDAR-independent LTP observed during the experiments of Perea and Araque (2007). There exists another model (Nadkarni et al. 2008) demonstrating the role of astrocytes on synaptic potentiation, but at that time a lot of important details were either undetermined (e.g., readily releasable pool size in astrocytes which has been determined recently by Malarkey and Parpura (2011)) or not modeled by them (e.g. post-synaptic neuron dynamics). A brief comparison between Nadkarni et al. (2008) and the proposed model is listed in Table 1. Nadkarni et al. (2008) made a commendable effort to reproduce the experimental findings of Kang et al. (1998) by coupling astrocyte Ca^{2+} activity with CA3 pyramidal neuron bouton through a heuristic coupling parameter. However, they did not take care of some important biological detail while modeling the TpS (see Appendix A where some of the aspects have been highlighted and compared with our proposed model).

Table 1 A comparison between Nadkarni et al. (2008) and our proposed model

Signaling Processes Modeled	Nadkarni et al. 2008	Proposed Model
Bouton Ca^{2+}	Yes	Yes
Bouton IP_3	No	Yes
Synaptic Vesicle/Glutamate	Yes/No	Yes/Yes
Astrocytic Ca^{2+}	Yes	Yes
Astrocytic IP_3	Yes	Yes
Extra-synaptic Vesicle/Glutamate	No/No	Yes/Yes
Post-Synaptic Current/Potential	Yes/No	Yes/Yes
Post-Synaptic Calcium/Buffer	No/No	Yes/Yes
Retrograde Signaling	No	Yes

2 The model

As mentioned in the previous section, the LTP we were trying to model is an NMDAR-independent LTP with purely pre-synaptic locus of induction. The exact mechanism underlying this phenomenon was not investigated by Perea and Araque (2007). However, as demonstrated by a persistent increase in Pr a plausible role of a retrograde messenger, possibly NO is suspected. NO is a retrograde messenger involved in different forms of synaptic plasticity (Garthwaite and Boulton 1995; Bon and Garthwaite 2003; Hopper and Garthwaite 2006; Phillips et al. 2008; Taqatqeh et al. 2009) that may be involved in the astrocyte-induced synaptic potentiation (Alfonso Araque personal communication). Here, in this section we present the mathematical model associated with the addressed biological problem, whose computational implementation will be presented in the section that follows. Since, Perea and Araque (2007) performed their experiments over immature wistar rats, attempt has been made to develop the model and collect data while keeping in mind immature cells. The mathematical formulations have been described in the subsequent subsections. The major steps involved are presented as a flowchart in Fig. 1.

2.1 Pre-synaptic action potential

Action potential (AP) is generated at the axon hillock of the pre-synaptic neuron in response to an applied current density of 10 $\mu A\ cm^{-2}$ and frequency 5 Hz. The classical HH (Hodgkin and Huxley 1952) paradigm has been used to generate pre-synaptic AP. Since in this paper our focus is not on the detail of the pre-synaptic AP generation, for the sake of simplicity, we have followed the HH model for the pre-synaptic regular spikes generation. Nadkarni and Jung (2003) also followed the HH model for generation of the pre-synaptic AP.

$$C\frac{dV_{pre}}{dt} = I_{app} - g_K n^4 (V_{pre} - V_K) - g_{Na} m^3 h (V_{pre} - V_{Na}) - g_L (V_{pre} - V_L)$$
$$\frac{dx}{dt} = \alpha_x (1 - x) - \beta_x x \tag{1}$$

where V_{pre} is pre-synaptic membrane potential, I_{app} is applied current density, g_K, g_{Na} and g_L are potassium, sodium and leak conductance respectively, V_K, V_{Na} and V_L are potassium,

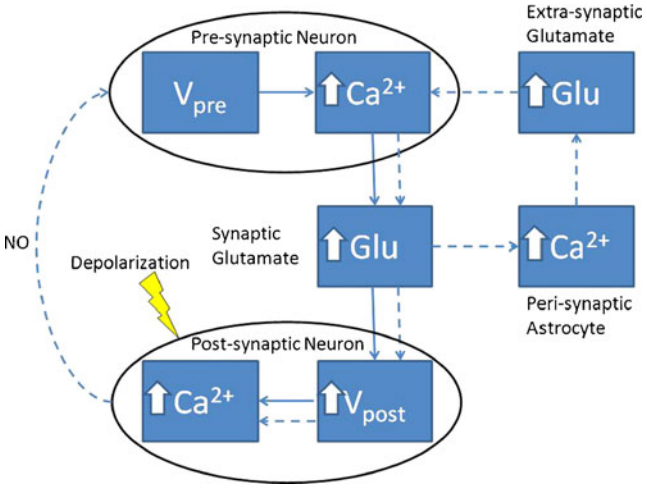

Fig. 1 Information flow from pre-synaptic neuron to post-synaptic neuron as modulated by a peri-synaptic astrocyte. Solid line represents astrocyte-independent pathway, while, solid line accompanied by broken line represents astrocyte-dependent pathway. 1) Pre-synaptic AP generated at axon hillock, 2) increased Ca^{2+} concentration in bouton due to opening of VGCCs, 3) elevated synaptic glutamate concentration due to exocytosis of synaptic vesicles –3(**a**) synaptic glutamate taken up by astrocytic mGluRs instigates the process of astrocyte Ca^{2+} oscillations –3(**b**) exocytosis of synaptic-like micro-vesicles (SLMVs) leading to an increase in extra-synaptic glutamate concentration; increased glutamate is free to diffuse and binds with mGluRs on the surface of pre-synaptic bouton leading to further flow of Ca^{2+} inside the bouton from intracellular stores responsible for increasing Ca^{2+} concentration transiently, 4) synaptic glutamate is also free to bind with post-synaptic glutamate receptors, (α-amino-3-hydroxy-5-methyl-4-isoxazolepropionic acid receptor) AMPAR here, which leads to an increase in post-synaptic membrane potential, 5) [Ca^{2+}] increase in spine due to fractional Ca^{2+}—current carried by AMPARs and opening of VGCCs during mild-depolarization of post-synaptic neuron. The retrograde signal (NO) denoted by dotted line is to denote its pervasiveness only in an astrocyte-dependent pathway of information processing. The mechanism underlying the proposed role of NO over enhancement of Pr is explained in subsection 2.10

sodium and leak reversal potential respectively, and $x=m$ (Na^+ activation), h (Na^+ inactivation) and n (K^+ activation). The detail of the HH model can be found in (Hodgkin and Huxley 1952). The values of the different parameters in equation (1) that have been used in this paper are furnished in the Table 2. α_x and β_x for $x=m$, h and n are defined as

$$\alpha_n = \frac{0.01(-V_{pre}-60)}{\exp(\frac{-V_{pre}-60}{10})-1}, \alpha_m = \frac{0.1(-V_{pre}-45)}{\exp(\frac{-V_{pre}-45}{10})-1},$$
$$\alpha_h = 0.07\exp(\frac{-V_{pre}-70}{20}), \beta_n = 0.125\exp(\frac{-V_{pre}-70}{80}),$$
$$\beta_m = 4\exp(\frac{-V_{pre}-70}{18}), \beta_h = \frac{1}{\exp(\frac{-V_{pre}-40}{10})+1}$$

2.2 Pre-synaptic bouton Ca^{2+} dynamics

Input to our mathematical model i.e. the train of AP generated at axon hillock, travels all the way down to the pre-synaptic axon end-feet (or bouton). Its invasion leads to opening of the voltage-gated Ca^{2+} channels (VGCCs), in particular the N-type Ca^{2+} channels, which have been shown to carry majority of the Ca^{2+} required for neurotransmitter release in immature neurons (Mazzanti and Haydon 2003; Weber et al. 2010). The total Ca^{2+} concentration, c_i, inside the bouton can be divided into two components:

i) Ca^{2+} concentration due to AP, denoted as c_{fast}, and
ii) Ca^{2+} concentration due to intracellular stores, c_{slow}.

Due to its rapid kinetics, the Ca^{2+} from the VGCCs is termed c_{fast}. Similarly, Ca^{2+} from the endoplasmic reticulum (ER) or the intracellular stores is termed c_{slow} due to its slow kinetics. Hence, c_i satisfies the following simple equation

$$c_i = c_{fast} + c_{slow} \Rightarrow \frac{dc_i}{dt} = \frac{dc_{fast}}{dt} + \frac{dc_{slow}}{dt} \quad (2)$$

The expression for $\frac{dc_{fast}}{dt}$ and $\frac{dc_{slow}}{dt}$ are given by equations (3) and (5) respectively. The sensitivity of the Ca^{2+}—sensor of a synaptic vesicle has been studied in detail at the giant Calyx of Held synapses (Schneggenburger and Neher 2000; Bollmann et al. 2000). It was reported that an intracellular Ca^{2+} concentration of ~10 μM is sufficient for neurotransmitter release (Schneggenburger and Neher 2000; Bollmann et al. 2000) in contrast to earlier estimate of ~100 μM (Neher 1998). The equation governing the c_{fast} consists of simple construction-destruction type formulism and is as follows (Keener and Sneyd 2009)

$$\frac{dc_{fast}}{dt} = \underbrace{-\frac{I_{Ca}\cdot A_{btn}}{z_{Ca}FV_{btn}} + J_{PMleak}}_{\text{construction}} \underbrace{-\frac{I_{PMCa}\cdot A_{btn}}{z_{Ca}FV_{btn}}}_{\text{destruction}} \quad (3)$$

Here, I_{Ca} is the Ca^{2+} current through the N-type channels, A_{btn} is the surface area of the bouton (calculated assuming the bouton to be spherical and using the average volume of a bouton at SC—CA1 synapse due to Koester and Sakmann 2000), z_{Ca} is the Ca^{2+} ion valence, F is the Faraday's constant, V_{btn} is the volume of the bouton. I_{PMCa} represents the current due to electrogenic plasma-membrane Ca^{2+} ATPase. This high affinity and low capacity pump has known capability to extrude excess of Ca^{2+} out of the cell and it has also been shown that it regulates excitatory

Table 2 Parameter values used in the HH model (all are from Hodgkin and Huxley 1952)

Symbol	Value
g_K	36 mS/cm^2
g_{Na}	120 mS/cm^2
g_L	0.3 mS/cm^2
V_K	-82 mV
V_{Na}	45 mV
V_L	-59.4 mV

synaptic transmission at SC–CA1 synapses (Jensen et al. 2007). To keep it simple, the basic Michaelis-Menton (MM) type formulism has been used for the Ca^{2+} efflux through it (Erler et al. 2004; Blackwell 2005). J_{PMleak} is the positive leak from the extracellular space into bouton, which makes sure that MM pump does not decrease cytosolic Ca^{2+} to 0 (Blackwell 2005).

The Ca^{2+} current through VGCCs has been assumed to obey the Ohm's law. The formulation of I_{Ca} follows the single protein level formulation, which is described elsewhere (Erler et al. 2004)

$$I_{Ca} = \rho_{Ca} m_{Ca}^2 \underbrace{g_{Ca}(V_{pre}(t) - V_{Ca})}_{\text{Single open channel}}$$

Here,ρ_{Ca} is the N-type channel protein density which determines the number of Ca^{2+} channels on the membrane of the bouton, g_{Ca} is the single N-type channel conductance, V_{Ca} is the reversal potential of Ca^{2+} ion determined by the Nernst equation (Keener and Sneyd 2009)

$$V_{Ca} = \frac{RT}{z_{Ca}F} \ln\left(\frac{c_{ext}}{c_i^{rest}}\right), \tag{4}$$

where R is the real gas constant, T is the absolute temperature, c_{ext} is the extracellular Ca^{2+} concentration, c_i^{rest} is the total intracellular Ca^{2+} concentration at rest. It is assumed that a single N-type channel consists of two-gates. m_{Ca} denotes the opening probability of a single gate. A single N-type channel is open only when both the gates are open. Hence, m_{Ca}^2 is the single channel open probability. The time dependence of the single channel open probability is governed by an HH-type formulation

$$\frac{dm_{Ca}}{dt} = \frac{(m_{Ca}^{\infty} - m_{Ca})}{\tau_{m_{Ca}}},$$

where m_{Ca}^{∞} is the Boltzmann-function fitted by Ishikawa et al. (2005) to the whole cell current of an N-type channel, m_{Ca}approaches its asymptotic value m_{Ca}^{∞} with a time constant $\tau_{m_{Ca}}$. The mathematical expression of other parameters used in equation (3) is as follows

$$I_{PMCa} = v_{PMCa}\frac{c_i^2}{c_i^2 + K_{PMCa}^2}, J_{PMleak} = v_{leak}(c_{ext} - c_i), m_{Ca}^{\infty} = \frac{1}{1 + \exp\left((V_{m_{Ca}} - V_{pre})/k_{m_{Ca}}\right)}$$

Here, v_{PMCa} is the maximum PMCa current density, determined through computer simulations, so that c_i is maintained at its resting concentration. All other parameter values used for simulation are listed in Table 3.

Although, the flux of Ca^{2+} from the endoplasmic reticulum (ER) is mainly controlled by two types of receptors (or Ca^{2+} channels) i) the inositol (1,4,5)-trisphosphate receptor (IP_3R) and ii) the ryanodine receptor (RyR) (Sneyd and Falcke 2005). We have assumed ER to have IP_3R alone, because it has been shown to modulate ganglionic LTP (Vargas et al. 2010). The inositol (1,4,5)-triphosphate (IP_3) is necessary for the release of Ca^{2+} through IP_3R (on the surface of the ER). It is produced when the glutamate (agonist) binds with the mGluR (receptor) and causes via G-protein link to phospholipase C (PLC), the cleavage of phosphotidylinositol (4,5)-bisphosphate (PIP_2) to produce IP_3 and diacylglycerol (DAG). We have used the conventional Li-Rinzel model (L-R model) (Li and Rinzel 1994) to formulate this slower Ca^{2+} signaling process. A few modifications were made to the L-R model. The L-R model assumes that, total intracellular concentration, c_0, is conserved and determines the ER Ca^{2+} concentration, c_{ER}, using the following relation

$$c_{ER} = \frac{(c_0 - c_i)}{c_1}.$$

Such an assumption is not valid in the present model because of the presence of membrane fluxes, namely, I_{Ca} and I_{PMCa}. Also, in the L-R model intracellular IP_3 concentration is used as a control parameter. This is not supposed to hold in an active TpS. Hence, two additional equations governing ER Ca^{2+} concentration and IP_3 concentration have been incorporated in the classical L-R model. The IP_3 production term was made glutamate dependent to study the effect of astrocytic Ca^{2+} over c_i. The mathematical model governing the c_{slow} dynamics is as follows

$$\begin{aligned}
\frac{dc_{slow}}{dt} &= -c_1 v_1 m_{\infty}^3 n_{\infty}^3 q^3 (c_i - c_{ER}) - \frac{v_3 c_i^2}{k_3^2 + c_i^2} - c_1 v_2 (c_i - c_{ER}),\\
\frac{dc_{ER}}{dt} &= -\frac{1}{c_1}\frac{dc_{slow}}{dt},\\
\frac{dp}{dt} &= v_g \frac{g_a^{0.7}}{k_g^{0.7} + g_a^{0.7}} - \tau_p (p - p_0),\\
\frac{dq}{dt} &= \alpha_q (1 - q) - \beta_q q.
\end{aligned} \tag{5}$$

With, $m_{\infty} = \frac{p}{p+d_1}, n_{\infty} = \frac{c_i}{c_i + d_5}, \alpha_q = a_2 d_2 \frac{p+d_1}{p+d_3}, \beta_q = a_2 c_i$. In equation (5), the first term on the right hand side of $\frac{dc_{slow}}{dt}$ denotes Ca^{2+} flux from ER to the intracellular space through IP_3R, second term is the Ca^{2+} flux pumped from the intracellular space into ER, third term is the leak of Ca^{2+} ions from ER to intracellular space. c_{ER} is the ER Ca^{2+} concentration, c_1 is the ratio of volume of ER to volume of bouton, v_1 is maximal IP_3R flux rate, v_2 is the maximal Ca^{2+} leak from ER to intracellular space, v_3 maximal Sarco-Endoplasmic Reticulum ATPase (SERCA) pump rate, p is the intracellular IP_3 concentration, g_a is the glutamate

Table 3 Parameters used for Bouton Ca^{2+} dynamics

Symbol	Description	Value	Reference
F	Faraday's constant	96487 C/mole	
R	Real gas constant	8.314 J/K	
T	Absolute Temperature	293.15 K	Temperature in Perea and Araque (2007)
z_{Ca}	Calcium valence	2	
A_{btn}	Surface area of bouton	1.24 μm^2	Koester and Sakmann 2000
V_{btn}	Volume of bouton	0.13 μm^3	Koester and Sakmann 2000
ρ_{Ca}	N-type channel density	3.2/μm^2	This paper[a]
g_{Ca}	N-type channel conductance	2.3 pS	Weber et al. 2010
V_{Ca}	Reversal potential of Ca^{2+} ion	125 mV	Calculated using equation (4)
v_{PMCa}	Maximum PMCa current	0.4 $\mu A/cm^2$	See text; Page No. 7
K_{PMCa}	Ca^{2+} concentration at which v_{PMCa} is halved	0.1 μM	Erler et al. 2004
v_{leak}	Maximum leak of Ca^{2+} through plasma membrane	2.66×10^{-6}/ms	See text; Page No. 6
c_i^{rest}	Resting Intracellular Ca^{2+} concentration	0.1 μM	
c_{ext}	External Ca^{2+} concentration	2 mM	Extracellular [Ca^{2+}] in Perea and Araque (2007)
V_{mCa}	Half-activation voltage of N-type Ca^{2+} channel	-17 mV	Ishikawa et al. 2005
k_{mCa}	Slope factor of N-type channel activation	8.4 mV	Ishikawa et al. 2005
$\tau_{m_{Ca}}$	N-type channel time constant	10 ms	Ishikawa et al. 2005
c_1	Ratio of ER volume to volume of Bouton	0.185	Shuai and Jung 2002
v_1	Maximum IP_3 receptor flux	30/s	See text; Page No. 9
v_2	Ca^{2+} leak rate constant	0.2374/s	See text; Page No. 9
v_3	SERCA maximal pump rate	90 μM/s	See text; Page No. 9
k_3	SERCA dissociation constant	0.1 μM	Jafri and Keizer 1995
d_1	IP_3 dissociation constant	0.13 μM	Shuai and Jung 2002
d_2	Inhibitory Ca^{2+} dissociation constant	1.049 μM	Shuai and Jung 2002
d_3	IP_3 dissociation constant	943.4 nM	Shuai and Jung 2002
d_5	Activation Ca^{2+} dissociation constant	82.34 nM	Shuai and Jung 2002
a_2	Inhibitory Ca^{2+} binding constant	0.2 μM/s	Shuai and Jung 2002
v_g	Maximum production rate of IP_3	0.062 μM/s	Nadkarni et al. 2008
k_g	Glutamate concentration at which v_g is halved	0.78 μM	Nadkarni et al. 2008
τ_p	IP_3 degradation constant	0.14/s	Nadkarni et al. 2008
p_0	Initial IP_3 concentration	0.16 μM	Nadkarni et al. 2008

[a] Determined through computer simulations so that the average Pr lies between 0.2–0.3 (when astrocyte is not stimulated) similar to the experiments of Perea and Araque (2007)

concentration in the extra-synaptic cleft, q is the fraction of activated IP_3R.

Most of the values of v_1, v_2, v_3 mentioned in literature are for closed-cell dynamics which is not the case here. Hence, the values of v_1, v_2, v_3 were fixed through computer simulation runs so that Ca^{2+} homeostasis is maintained inside the bouton and its organelles with or without pre-synaptic stimulus. Details of parameters are as listed in Table 3.

2.3 Glutamate release dynamics in bouton

The sensitivity of the Ca^{2+}—sensor is a critical parameter which decides the release of glutamate from the synaptic vesicles. The study of Ca^{2+} sensitivity of the Ca^{2+}—sensor at hippocampal synapses is hampered due to its small size (Wang et al. 2009). However, Ca^{2+} sensitivity of the Ca^{2+}—sensor has been studied in detail at the giant Calyx of Held synapses (Schneggenburger and Neher 2000; Bollmann et al. 2000) and squid giant synapse (Llinas 1999). Schneggenburger and Neher (2000) suggested that an intracellular Ca^{2+} concentration of ~10 μM is sufficient for the neurotransmitter release at the giant Calyx of Held synapses. This estimate is 10 folds smaller than our estimate for hippocampal synapses i.e. 100 μM (Neher 1998; Nadkarni et al. 2008). The tour-de-force attempt (Schneggenburger and Neher 2000; Bollman et al. 2000) at the Calyx of Held is not easy to implement at small nerve terminals of hippocampal synapses. We have assumed the sensitivity of the Ca^{2+}—sensor to be the same as that of the

Calyx of Held. The kinetic model governing the Ca^{2+} binding to the Ca^{2+} sensor is given by the following equations (Bollmann et al. 2000)

$$X \underset{\beta}{\overset{5\alpha c_i}{\rightleftarrows}} X(c_i)_1 \underset{2\beta}{\overset{4\alpha c_i}{\rightleftarrows}} X(c_i)_2 \underset{3\beta}{\overset{3\alpha c_i}{\rightleftarrows}} X(c_i)_3 \underset{4\beta}{\overset{2\alpha c_i}{\rightleftarrows}} X(c_i)_4 \underset{5\beta}{\overset{\alpha c_i}{\rightleftarrows}} X(c_i)_5 \underset{\delta}{\overset{\gamma}{\rightleftarrows}} X(c_i)_5^*, \tag{6}$$

where, α and β are the Ca^{2+} association and dissociation rate constants respectively, γ and δ are Ca^{2+} independent isomerisation constants. X is the Ca^{2+} sensor, of a synaptic vesicle, with no Ca^{2+} bound, $X(c_i)_1$ is Ca^{2+} sensor with one Ca^{2+} bound, likewise $X(c_i)_5$ is the Ca^{2+} sensor with five Ca^{2+} bound and $X(c_i)_5^*$ is the isomer of $X(c_i)_5$ which is ready for glutamate release. Hippocampal synapses are known as low-fidelity synapses (Nadkarni et al. 2008). We have assumed an active zone consisting of two-docked synaptic vesicles (Danbolt 2001; Nikonenko and Skibo 2006). Since there are fewer synaptic vesicles, the number of vesicles with 5 Ca^{2+} ions bound cannot be determined by the average of vesicle pool. Therefore the fraction of the docked vesicles ready to be released f_r, has been determined using dynamic Monte-Carlo simulations (Fall et al. 2002) of kinetic equation (6) and depends on the $X(c_i)_5^*$ state.

Apart from the evoked release of glutamate, the spontaneous release of glutamate can also occur in our model. It is known that spontaneous release of neurotransmitter depends upon the pre-synaptic Ca^{2+} concentration (Emptage et al. 2001; Nadkarni et al. 2008). Also, it is known that the spontaneous release takes place when pre-synaptic Ca^{2+} is low i.e. when pre-synaptic membrane is not depolarized (Atluri and Regehr 1998; Hagler and Yukiko Goda 2001). The fraction of synaptic vesicles ready to be release spontaneously, f_r, is assumed to be a Poisson process with the following rate

$$\lambda(c_i) = a_3 \left(1 + \exp\left(\frac{a_1 - c_i}{a_2}\right)\right)^{-1}. \tag{7}$$

The formulation for the rate of spontaneous release is from Nadkarni et al. (2008). However, we have to modify the parameter values, in equation (7), because as per their choice of values and system setup, the frequency of spontaneously released vesicles was as high as 19 per sec (determined through simulation runs for over 10000 times). However, the experimentally determined frequency of spontaneous vesicle release in presence of an astrocyte is in between 1–3 per sec (Kang et al. 1998). Thus, we determined the values of a_1, a_2 and a_3 so that the frequency of spontaneous vesicle release is between 1–3 Hz. The vesicle fusion and recycling process is governed by the Tsodyks & Markram model (Tsodyks and Markram 1997). A slight modification has been made to the Tsodyks & Markram Model (TMM) to make the vesicle fusion process f_r dependent. The modified TMM is as follows

$$\begin{aligned} \frac{dR}{dt} &= \frac{I}{\tau_{rec}} - f_r \cdot R \\ \frac{dE}{dt} &= -\frac{E}{\tau_{inact}} + f_r \cdot R \\ I &= 1 - R - E \end{aligned} \tag{8}$$

where R is the fraction of the releasable vesicles inside the bouton, E is the fraction of the effective vesicles in the synaptic cleft and I is the fraction of the inactive vesicles undergoing recycling process, f_r has the value (0, 0.5, 1) provided that the pre-synaptic membrane is depolarized (for evoked vesicle release) or pre-synaptic membrane is not depolarized (for spontaneous vesicle release), corresponding to the number of vesicles ready to be released (0, 1, 2), which is determined by the stochastic simulation of the kinetic model in equation (6) (for evoked vesicle release) or generating a Poisson random variable with the rate given by equation (7) (for spontaneous vesicle release). τ_{inact} and τ_{rec} are the time constants of vesicle inactivation and recovery respectively. Once a vesicle is released whether evoked or spontaneous, the vesicle release process remains inactivated for a period of 6.34 ms (Nadkarni et al. 2008). The parametric values used for simulation are listed in Table 4.

Table 4 Parameters used for Glutamate dynamics in bouton and cleft

Symbol	Description	Value	Reference
α	Ca^{2+} association rate constant	0.3/μM ms	Bollman et al. 2000
β	Ca^{2+} dissociation rate constant	3/ms	Bollman et al. 2000
γ	Isomerization rate constant (forward)	30/ms	Bollman et al. 2000
δ	Isomerization rate constant (backward)	8/ms	Bollman et al. 2000
τ_{rec}	Vesicle recovery time constant	800 ms	Tsodyks and Markram 1997
τ_{inac}	Vesicle inactivation time constant	3 ms	Tsodyks and Markram 1997
a_1	Ca^{2+} concentration at which λ is halved	50 μM	See text; Page No. 11
a_2	Slope factor of spontaneous release rate λ	5 μM	See text; Page No. 11
a_3	Maximum spontaneous release rate	0.85/ms	See text; Page No. 11
n_v	Number of docked vesicle	2	Nikonenko and Skibo 2006
g_v	Glutamate concentration in single vesicle	60 mM	Montana et al. 2006
g_c	Glutamate clearance rate constant	10/ms	Destexhe et al. 1998

2.4 Glutamate dynamics in synaptic cleft

The effective concentration of glutamate in the synaptic cleft is decisive in controlling synaptic efficacy unless the post-synaptic receptors are already saturated which is possible in response to a high frequency stimulus (HFS). In our model, the glutamate available in the synaptic cleft was made available to the post-synaptic receptors and mGluR on the surface of astrocyte. Since E gives the effective fraction of the vesicles in the synaptic cleft, the estimated glutamate concentration in synaptic cleft can be represented mathematically as

$$\frac{dg}{dt} = n_v \cdot g_v \cdot E - g_c \cdot g \tag{9}$$

Here g is the glutamate concentration in the synaptic cleft, n_v is the number of docked vesicle, g_v is the vesicular glutamate concentration and g_c is the rate of glutamate clearance i.e., re-uptake by neuron or astrocyte. Using this simple dynamics we could achieve the estimated range of glutamate concentration 0.24–11 mM in synaptic cleft (Danbolt 2001; Franks et al. 2002) and time course of glutamate in synaptic cleft 2 ms (Franks et al. 2002; Nadkarni and Jung 2007). Although a similar equation can be used to model the glutamate dynamics in other synapses, although, one may have to use different constant values. Thus the present formulation can be considered specific to the SC—CA1 synapse.

2.5 Astrocyte Ca^{2+} dynamics

Porter and McCarthy (1996) demonstrated that the glutamate released from the SC leads to an increase in astrocytic Ca^{2+} via an mGluR-dependent pathway in situ. Also recently De Pittà et al. (2009) proposed a mathematical model, termed as G-ChI, for astrocytic Ca^{2+} concentration increase through an mGluR-dependent pathway. They used glutamate as a stimulating parameter to evoke increases in astrocytic Ca^{2+} concentration, while in our model glutamate comes through SC in an activity-dependent manner (see equation (9)). The G-ChI model uses the conventional L-R model for astrocytic Ca^{2+} concentration 'c_a' with some specific terms for the astrocytic IP_3 concentration 'p_a.' The model incorporates PLCβ and PLCδ dependent IP_3 production. It also incorporates inositol polyphosphate 5-phosphatase (IP-5P) and IP_3 3-kinase (IP_3-3 K) dependent IP_3 degradation (for details see De Pittà et al. 2009). It is a very detailed, astrocyte specific, model which exhibits IP_3 oscillations apart from Ca^{2+} oscillations. However the exact significance of IP_3 oscillation is not yet known (De Pittà et al. 2009). The G-ChI model is a closed-cell model (Keener and Sneyd 2009) i.e. without membrane fluxes. In such models c_a primarily depends upon two parameters namely, i) flux from ER into cytosol and ii) the maximal pumping capacity of the SERCA pump. IP_3R is found in clusters of variable size (Nadkarni and Jung 2007). The exact size of cluster is supposed to vary from cell to cell but following Nadkarni and Jung (2007) we have assumed it be 20. Considering such a small size of IP_3R cluster stochasticity does play a significant role (see Shuai and Jung 2002), and hence instead of using an ordinary differential equation for gating parameter h_a, we have used Langevin equation (Fox 1997; Shuai and Jung 2002). The model can be represented as follows

$$\frac{dc_a}{dt} = -r_{c_a} m_{\infty,a}^3 n_{\infty,a}^3 h_a^3 \left(c_0 - \left(1 + c_{1,a}\right) c_a\right) - v_{ER} \frac{c_a^2}{c_a^2 + K_{ER}^2} - r_L \left(c_0 - \left(1 + c_{1,a}\right) c_a\right) \tag{10}$$

$$\frac{dp_a}{dt} = v_\beta \cdot \mathrm{Hill}\left(g^{0.7}, K_R\left(1 + \frac{K_p}{K_R}\mathrm{Hill}(C, K_\pi)\right)\right) + \frac{v_\delta}{1 + \frac{p_a}{k_\delta}}\mathrm{Hill}\left(c_a^2, K_{PLC\delta}\right) + v_{3K}\mathrm{Hill}\left(c_a^4, K_D\right)\mathrm{Hill}\left(p_a, K_3\right) - r_{5p_a} p_a \tag{11}$$

$$\frac{dh_a}{dt} = \alpha_{h_a}(1 - h_a) - \beta_{h_a} h_a + G_h(t) \tag{12}$$

The first term on the right hand side of equation (10) is due to efflux of Ca^{2+} from ER to intracellular space, the second term represents removal of excess Ca^{2+} from intracellular space in to ER by the SERCA pump, the third term is a constant leak of Ca^{2+} concentration from ER to intracellular space. r_{c_a} is the maximal rate of Ca^{2+} flux from ER, $m_{\infty,a}^3 \cdot n_{\infty,a}^3 \cdot h_a^3$ governs the opening probability of the IP_3R cluster, c_0 is the cell-averaged total of the free Ca^{2+} concentration, $c_{1,a}$ is the ratio of ER and cytosol volume, v_{ER} is the maximal rate of Ca^{2+} uptake by the SERCA pump, K_{ER} is the SERCA pump Ca^{2+} affinity, r_L is the maximal rate of Ca^{2+} leakage from the ER. The first two terms on the right hand side of equation (11) are IP_3 producing terms due to PLCβ and PLCδ respectively; the last two terms are IP_3 degradation terms due to IP_3-3 K and IP-5P respectively (for a systematic derivation, see De Pittà et al. (2009)). Equation (12) is analogous to gating variable q in equation (5) except for $G_h(t)$, which is a zero mean, uncorrelated, Gaussian white-noise term with co-variance function (Nadkarni and Jung 2007)

$$\langle G_h(t) G_h(t') \rangle = \frac{\alpha_{h_a}(1 - h_a) + \beta_{h_a} h_a}{N_{IP_3}} \delta(t - t')$$

Here, $\delta(t)$ is the Dirac-delta function, t and t' are time and $\frac{\alpha_{h_a}(1-h_a)+\beta_{h_a} h_a}{N_{IP_3}}$ is the spectral density (Coffey et al. 2005).

Mathematical expression of all other parameters in equations (10)–(12) are

$$m_{\infty,\mathrm{a}} = \mathrm{Hill}(p_\mathrm{a}, d_1), n_{\infty,\mathrm{a}} = \mathrm{Hill}(c_\mathrm{a}, d_5), \mathrm{Hill}(x^n, K) = \frac{x^n}{x^n + K^n},$$
$$\alpha_{h_\mathrm{a}} = a_2 d_2 \frac{p_\mathrm{a} + d_1}{p_\mathrm{a} + d_3}, \beta_{h_\mathrm{a}} = a_2 c_\mathrm{a}$$

Hill(x^n,K) is the generic Hill function (De Pittà et al. 2009). Hill function is generally used to model those reactions whose reaction velocity curve is not hyperbolic (Keener and Sneyd 2009). Details of all parameters are as listed in Table 5.

2.6 Gliotransmitter release dynamics in astrocyte

Astrocytes *in vitro* and *in vivo* have been shown to contain synaptic-like micro-vesicles (SLMVs) (Bezzi et al. 2004; Marchaland et al. 2008) and express the protein machinery necessary for Ca^{2+}-dependent exocytosis process (Bezzi et al. 2004; Montana et al. 2006; Verkhratsky and Butt 2007; Parpura and Zorec 2010). However, the exact mechanism by which astrocyte release gliotransmitter is yet to be determined (Wenker 2010; Ben Achour et al. 2010). Parpura and Haydon (2000) determined Ca^{2+} dependency of glutamate release from the hippocampal astrocytes. In their study the Hill coefficient for glutamate release was 2.1–2.7 suggesting at least two Ca^{2+} ions are must for a possible gliotransmitter release (Parpura and Haydon 2000). Following the experimental observation of Parpura and Haydon (2000), in this manuscript, it has been assumed that the binding of three Ca^{2+} ions to an SLMV makes it fusogenic (ready to be released). The percent of fusogenic SLMVs in response to a mechanical stimulation and the size of readily releasable pool of SLMVs in the astrocytes have been determined recently (Malarkey and Parpura 2011). It is assumed that the gliotransmitter release site contains three independent gates (S_1–S_3), for the three Ca^{2+} ions to bind, with different opening and closing constants. The model governing the gliotransmitter release site activation is based on Bertram et al. (1996) and is as follows

$$c_\mathrm{a} + C_\mathrm{j} \underset{k_\mathrm{j}^-}{\overset{k_\mathrm{j}^+}{\rightleftarrows}} O_\mathrm{j} \qquad \mathrm{j} = 1, 2, 3$$

Where, k_j^+andk_j^- are the opening and closing rates of the gate 'S_j'; C_j and O_j are the closing and opening probability of the gate S_j. The temporal evolution of the open gate 'O_j' can be expressed as

$$\frac{dO_\mathrm{j}}{dt} = k_\mathrm{j}^+ \cdot c_\mathrm{a} - \left(k_\mathrm{j}^+ \cdot c_\mathrm{a} + k_\mathrm{j}^-\right) \cdot O_\mathrm{j} \tag{13}$$

Table 5 Parameters used for astrocyte Ca^{2+} dynamics

Symbol	Description	Value	Reference
r_{c_a}	Maximal IP_3R flux	6/s	De Pittà et al. 2009
r_L	Maximal rate of Ca^{2+} leak from ER	0.11/s	De Pittà et al. 2009
c_0	Total cell free Ca^{2+} concentration	2 μM	De Pittà et al. 2009
$c_{1,\mathrm{a}}$	Ratio of ER volume to cytosol volume	0.185	De Pittà et al. 2009
v_{ER}	Maximal rate of SERCA uptake	0.9 μM/s	De Pittà et al. 2009
K_{ER}	SERCA Ca^{2+} affinity	0.1 μM	De Pittà et al. 2009
d_1	IP_3 dissociation constant	0.13 μM	De Pittà et al. 2009
d_2	Ca^{2+} inactivation dissociation constant	1.049 μM	De Pittà et al. 2009
d_3	IP_3 dissociation constant	0.9434 μM	De Pittà et al. 2009
d_5	Ca^{2+} activation dissociation constant	0.08234 μM	De Pittà et al. 2009
a_2	IP_3R binding rate for Ca^{2+} Inhibition	2/s	De Pittà et al. 2009
N	Number of IP_3R in a cluster	20	Nadkarni and Jung 2007
Glutamate-dependent IP_3 production			
v_β	Maximal rate of IP_3 production by PLCβ	0.5 μM/s	De Pittà et al. 2009
K_R	Glutamate affinity of the receptor	1.3 μM	De Pittà et al. 2009
K_p	Ca^{2+}/PKC-dependent inhibition factor	10 μM	De Pittà et al. 2009
K_π	Ca^{2+} affinity of PKC	0.6 μM	De Pittà et al. 2009
Glutamate-independent IP_3 production			
v_δ	Maximal rate of IP_3 production by PLCδ	0.05 μM/s	De Pittà et al. 2009
$K_{\mathrm{PLC}\delta}$	Ca^{2+} affinity of PLCδ	0.1 μM	De Pittà et al. 2009
k_δ	Inhibition constant of PLCδ activity	1.5 μM	De Pittà et al. 2009
IP_3 degradation			
r_{5pa}	Maximal rate of degradation by IP-5P	0.05/s	De Pittà et al. 2009
v_{3K}	Maximal rate of degradation by IP_3-3 K	2 μM/s	De Pittà et al. 2009
K_D	Ca^{2+} affinity of IP_3-3 K	0.7 μM	De Pittà et al. 2009
K_3	IP_3 affinity of IP_3-3 K	1 μM	De Pittà et al. 2009

An SLMV is ready to be released when all three gates are bound with Ca^{2+}. Hence, the probability that an SLMV is ready to be released is given by

$$f_\mathrm{r}^\mathrm{a} = O_1 \cdot O_2 \cdot O_3. \tag{14}$$

The dissociation constants of gates S_1–S_3 are 108 nM, 400 nM, and 800 nM. The time constants for gate closure $\left(1/k_j^-\right)$ are 2.5 s, 1 s, and 100 ms, respectively. The

dissociation constants and time constants for S_1 and S_2 are same as in Bertram et al. (1996). While the dissociation constant and time constant for gate S_3 were fixed through computer simulations to fit the experimentally determined probability of fusogenic SLMVs found recently (Malarkey and Parpura 2011). Similar to pre-synaptic bouton, the SLMV fusion and recycling process is modeled using TMM after making the release process f_r^a dependent. The governing model is as follows

$$\begin{aligned}\frac{dR_a}{dt} &= \frac{I_a}{\tau_{rec}^a} - \Theta\left(c_a - c_a^{thresh}\right)\cdot f_r^a \cdot R_a \\ \frac{dE_a}{dt} &= -\frac{E_a}{\tau_{inact}^a} + \Theta\left(c_a - c_a^{thresh}\right)\cdot f_r^a \cdot R_a \\ I_a &= 1 - R_a - E_a\end{aligned} \tag{15}$$

Here R_a is the fraction of the readily releasable SLMV inside the astrocyte, E_a is the fraction of the effective SLMV in the extra-synaptic cleft and I_a is the fraction of the inactive SLMV undergoing endocytosis or re-acidification process. Θ is the Heaviside function and c_a^{thresh} is the threshold of astrocyte Ca^{2+} concentration necessary for release site activation (Parpura and Haydon 2000). τ_{inact}^a and τ_{rec}^a are the time constants of inactivation and recovery respectively.

2.7 2.7 Glutamate dynamics in extra-synaptic cleft

The glutamate in the extra-synaptic cleft g_a, has been modeled in a similar way to equation (9). This glutamate acts on extra-synaptically located group I mGluR of the pre-synaptic bouton. It is used as an input in the IP_3 production term of equation (5). The SLMVs of the astrocytes are not as tightly packed as in neurons (Bezzi et al. 2004). Thus it is assumed that each SLMV contains 20 mM of glutamate (Montana et al. 2006). The mathematical equation governing the glutamate dynamics are as follows

$$\frac{dg_a}{dt} = n_a^v \cdot g_a^v \cdot E_a - g_a^c \cdot g_a, \tag{16}$$

where g_a is the glutamate concentration in the extra-synaptic cleft, n_a^v represents the size of readily releasable pool of SLMVs, g_a^v is the glutamate concentration in one SLMV, g_a^c is the clearance rate of glutamate from the cleft due to diffusion and/or re-uptake.

2.8 Post-synaptic membrane potential

The dendritic spine-head is assumed to be of mushroom type. Its volume is taken to be 0.9048 μm^3 (assuming a spherical spine-head of radius 0.6 μm (Dumitriu et al. 2010)). The specific capacitance and specific resistance of the spine-head is assumed to be 1 $\mu F/cm^2$ and 10000 Ω cm^2, respectively (Koch 1999). The spine-neck is assumed to be of negligible diameter. Given the size of the spine we can calculate its actual resistance as

$$R_m = \frac{R_M}{A_{spine}} \tag{17}$$

Where, R_m is actual resistance, R_M is specific resistance and A_{spine} is the area of spine-head. NMDAR and AMPAR are co-localized in most of the glutamatergic synapses, most of which are found in dendrite spines (Franks et al. 2002). Since we were modeling NMDAR-independent LTP hence NMDAR was not mathematically modeled. The post-synaptic potential change has been modeled using a passive membrane mechanism (Tsodyks and Markram 1997)

$$\tau_{post}\frac{dV_{post}}{dt} = -(V_{post} - V_{post}^{rest}) - R_m \cdot (I_{soma} + I_{AMPA}), \tag{18}$$

where τ_{post} is the post-synaptic membrane time constant, V_{post}^{rest} is the post-synaptic resting membrane potential, I_{soma} is the current injected in soma to raise the post-synaptic potential to -30 mV, I_{AMPA} is the AMPAR current and is given by the following expression

$$I_{AMPA} = g_{AMPA} m_{AMPA}\left(V_{post} - V_{AMPA}\right) \tag{19}$$

where g_{AMPA} is the conductance of the AMPARs at single synapses, V_{AMPA} is the reversal potential of the AMPAR and m_{AMPA} is the gating variable of AMPAR. Although there exist more comprehensive and detailed models for AMPAR gating (Destexhe et al. 1998) we have used a simple 2-state model to avoid redundant complexity. The simple 2-state model is known to retain most of the important qualitative properties of AMPAR (Destexhe et al. 1998). AMPAR gating is governed by the following HH-type formulism (Destexhe et al. 1998)

$$\frac{dm_{AMPA}}{dt} = \alpha_{AMPA} g(1 - m_{AMPA}) - \beta_{AMPA} m_{AMPA}$$

Here α_{AMPA} is the opening rate of the receptor, β_{AMPA} is the closing rate of the receptor and g is the glutamate concentration in the cleft given by equation (9). The parameter values are as listed in Tables 6 and 7.

2.9 Post-synaptic Ca^{2+} dynamics

The primary source of Ca^{2+} in spines is NMDARs or VGCCs (Keller et al. 2008). In our model, there is no NMDAR present, hence the primary source of the Ca^{2+} is the VGCC. Pharmacological analysis suggests that CA1 spines contain mostly R-type Ca^{2+} channels (Sabatini et al. 2001; Bloodgood and Sabatini 2007). Thus it is the only type of VGCC present on the surface of a spine-head in our model. AMPAR with missing GluR2-subunit are also permeable to Ca^{2+}. It has been reported that 1.2–1.3 % of the current carried

Table 6 Parameters used for Glutamate dynamics in astrocyte and extra-synaptic cleft

Symbol	Description	Value	Reference
k_1^+	Ca^{2+} association rate for S_1	3.75×10^{-3}/μM ms	Bertram et al. 1996
k_1^-	Ca^{2+} dissociation rate for S_1	4×10^{-4}/ms	Bertram et al. 1996
k_2^+	Ca^{2+} association rate for S_2	2.5×10^{-3}/μM ms	Bertram et al. 1996
k_2^-	Ca^{2+} dissociation rate for S_2	1×10^{-3}/ms	Bertram et al. 1996
k_3^+	Ca^{2+} association rate for S_3	1.25×10^{-2}/μM ms	See text; Page No. 15
k_3^-	Ca^{2+} dissociation rate for S_3	1×10^{-3}/ms	See text; Page No. 15
τ_{rec}^a	Vesicle recovery time constant	800 ms	Tsodyks and Markram 1997
τ_{inac}^a	Vesicle inactivation time constant	3 ms	Tsodyks and Markram 1997
c_a^{thresh}	Astrocyte response threshold	196.69 nM	Parpura and Haydon 2000
n_a^v	SLMV ready to be released	12	Malarkey and Parpura 2011
g_a^v	Glutamate concentration in one SLMV	20 mM	Montana et al. 2006
g_a^c	Glutamate clearance rate from the extra-synaptic cleft	10/ms	Destexhe et al. 1998

by AMPAR is Ca^{2+} current (Schneggenburger et al. 1993; Bollmann et al. 1998). It is supposed that AMPAR is the only other source of Ca^{2+} apart from VGCC. Apart from the above mentioned Ca^{2+} sources, the effect of endogenous Ca^{2+} buffers has also been incorporated in our model. These buffers are known to have a low buffering capacity of 20 units, which means ~5 % Ca^{2+} entering remains unbound (Helmchen 2002). The buffering capacity of the endogenous buffers in our model is also 20 units. In fact, the endogenous buffer in our model is calmodulin, which binds with the cytosolic Ca^{2+} to regulate the phosphorylation and the autophosphorylation of Ca^{2+}/calmodulin-dependent protein kinase (CaM-KII) which has been modeled in the next section.

Ca^{2+} extrusion is supposed to be carried out with the help of the PMCa pump. The loss of the Ca^{2+} due to the diffusion has not been considered (because of negligible diameter of neck). The reaction between Ca^{2+} and endogenous buffer is modeled using the following bi-molecular reaction

$$c_{post} + b \underset{k_b}{\overset{k_f}{\rightleftarrows}} c_{post} \cdot b. \tag{20}$$

Here k_f and k_b are the forward and backward rate constants respectively, c_{post} represents the post-synaptic spine Ca^{2+} concentration, b represents the free buffer concentration and $c_{post}\cdot b$ represents bound Ca^{2+} concentration. There are no sources or sinks for endogenous buffers. The reactions in equation (20) can be represented in the form of the following system of ordinary differential equations

$$\frac{dc_{post}}{dt} = f\left(c_{post}\right) - k_f c_{post}(b_t - c_{post}\cdot b) + k_b c_{post}\cdot b \tag{21}$$

$$\frac{dc_{post}\cdot b}{dt} = k_f c_{post}(b_t - c_{post}\cdot b) - k_b c_{post}\cdot b, \tag{22}$$

Here $f(c_{post})$ is the Ca^{2+} due to the membrane influx and efflux and b_t is the total endogenous buffer concentration. If we assume buffering kinetics to be fast, then we can take $c_{post}\cdot b$ to be in quasi-steady state i.e., $k_f c_{post}(b_t - c_{post}\cdot b) - k_b c_{post}\cdot b = 0$, and solving for $c_{post}\cdot b$ we get (Higgins et al. 2006)

$$c_{post}\cdot b = \frac{b_t c_{post}}{K_{endo} + c_{post}}, K_{endo} = \frac{k_b}{k_f},$$

Then the total Ca^{2+} concentration inside spine will be

$$\frac{dc_{post}}{dt} + \frac{dc_{post}\cdot b}{dt} = (1+\theta)\frac{dc_{post}}{dt} = f\left(c_{post}\right) \tag{23}$$

Where, $\theta = \frac{b_t K_{endo}}{(K_{endo}+c_{post})^2}$. The value of K_{endo} has been taken to be that of calmodulin and b_t was chosen so that the

Table 7 List of parameters used for post-synaptic potential generation

Symbol	Description	Value	Reference
R_m	Actual resistance of the spine-head	0.7985×10^5MΩ	Calculated using equation (17)
V_{post}^{rest}	Post-synaptic resting membrane potential	-70 mV	
τ_{post}	Post-synaptic membrane time constant	50 ms	Tsodyks and Markram 1997
g_{AMPA}	AMPAR conductance	0.35 nS	Destexhe et al. 1998
V_{AMPA}	AMPAR reversal potential	0 mV	Destexhe et al. 1998
α_{AMPA}	AMPAR forward rate constant	1.1 μM/s	Destexhe et al. 1998
β_{AMPA}	AMPAR backward rate constant	190/s	Destexhe et al. 1998

buffering factor (1+θ) becomes 20 units i.e., equal to the buffering factor of endogenous buffers (Helmchen 2002). Buffering effect, over post-synaptic Ca^{2+} concentration, is approximated by division by the buffering factor

$$\frac{dc_{\text{post}}}{dt} = \frac{f\left(c_{\text{post}}\right)}{1+\theta}. \tag{24}$$

As we know $f(c_{\text{post}})$ includes membrane proteins, VGCC and PMCa responsible for the Ca^{2+} influx and efflux. The Ca^{2+} current through VGCC is linear for the range of voltages in spines (-65 mV to -3 mV; Keller et al. 2008). We have assumed 12 VGCCs at the surface of spine, which is consistent with experimental estimates at the spine (1–20 VGCCs; Sabatini and Svoboda 2000). Sabatini and Svoboda (2000) determined the mean open probability P_{open} of the VGCC following a dendritic AP. Also in a spine containing N channels, which opens with the probability P_{open} per action potential, the number of channels opened by an action potential is governed by the binomial distribution (Katz and Miledi 1970). Thus to determine the number of VGCCs open, we generated a binomially-distributed random number (BRN) whenever V_{post} is greater than activation threshold of R-type channel i.e.–30 mV (Berridge 2009). The Ca^{2+} current through the ensemble of R-type channels is

$$i_{\text{R}} = g_{\text{R}} B\left(N, P_{\text{open}}\right)\left(V_{\text{post}} - V_{\text{R}}\right). \tag{25}$$

Here g_{R} is the conductance of a single R-type channel, $B(N,P_{\text{open}})$ is the binomially distributed random variable determining the number of R-type channels open following post-synaptic neuron depolarization to -30 mV, V_{R} is the reversal potential of hippocampal neuron R-type channel current determined by Sochivko et al. (2002). The efflux through PMCa is taken to be of the following form

$$s_{\text{pump}} = k_{\text{s}}\left(c_{\text{post}} - c_{\text{post}}^{\text{rest}}\right). \tag{26}$$

Here $c_{\text{post}}^{\text{rest}}$ is the resting post-synaptic Ca^{2+} concentration, k_{s} is the maximum rate of Ca^{2+} ion efflux due to the PMCa. Thus

$$f\left(c_{\text{post}}\right) = -\frac{(\eta I_{\text{AMPA}} + i_{\text{R}})}{z_{\text{Ca}} F V_{\text{spine}}} - s_{\text{pump}}, \tag{27}$$

where η is the fractional Ca^{2+} current carried by AMPAR, V_{spine} is the volume of the spine-head, I_{AMPA}, i_{R}, s_{pump} are given by equation (19), equations (25)–(26). All other parameters are as stated in Table 8.

2.10 Post-synaptic CaM-KII phosphorylation

CaM-KII is a Ca^{2+}-activated protein kinase with switch-like properties (Griffith 2004). CaM-KII consists of 8–12 subunits that form a petal structure (Zhabotinsky 2000). The analysis of CaM-KII autophosphorylation and dephosphorylation indicate that it can serve as a molecular switch which is capable of long-term memory storage (Lisman et al. 2002). The role of CaM-KII autophosphorylation in induction of LTP is well accepted while its role in LTP maintenance is still an open question (Zhabotinsky 2000). Phosphorylation of AMPAR by activated CaM-KII at Serine–831 (or Ser^{831} is a residue of the GluR1 subunit of AMPAR) is the most observed form of LTP (Lee et al. 2003; Boehm and Malinow 2005). The LTP we are trying to model does not involve the role of CaM-KII in phosphorylation of the AMPAR, as Perea and Araque (2007) observed no change in synaptic potency. The locus of induction of LTP observed by Perea and Araque (2007) was purely pre-synaptic requiring mild-depolarization of the post-synaptic neuron signifying the possible role of a retrograde messenger. NO might be the elusive retrograde messenger involved because of its demonstrated capability in regulating LTP at hippocampus (Bon and Garthwaite 2003; Hopper and Garthwaite 2006). Neuronal nitric oxide synthase (nNOS) enzyme is responsible for the production of NO inside the CNS (Calabrese et al. 2007). The production of NO from nNOS is known to be Ca^{2+} and calmodulin dependent (Garthwaite and Boulton 1995). Recently it has been demonstrated that CaM-KII phosphorylation leads to NO production from NOS in endothelial cells (Ching et al. 2011). Also, both nNOS and CaM-KII coexist in the post-synaptic density (or PSD is a neuronal scaffolding protein that associates with post-synaptic membrane receptors and links them to intracellular signaling molecules, like kinases and phosphatases) (Nikonenko et al. 2008) therefore a possible role of CaM-KII in NO production from nNOS cannot be overlooked. It is interesting to note that phosphorylation of nNOS at residue Serine-847 (Ser^{847}) by CaM-KII can decrease NO production in neuron cells (Watanabe et al. 2003) but phosphorylation of nNOS at residue Serine-1412 (Ser^{1412}) increases NO production (Rameau et al. 2007). Rameau et al. (2007) demonstrated, with the help of *okadaic acid* a protein phosphatase 1 (PP1) inhibitor, that the phosphorylated CaM-KII may reduce dephosphorylation of nNOS at Ser^{1412} and hence contribute in the NO production.

Based on the experimental observations discussed in the above paragraph, we infer that the Ca^{2+} entering inside the post-synaptic spine-head through VGCC and AMPAR (as described in section 2.9) leads to phosphorylation of CaM-KII. This phosphorylated CaM-KII stimulates the production of NO from nNOS (McCue et al. 2010; Forstermann and Sessa 2011). The produced NO is free to diffuse to the pre-synaptic terminal where it causes an increase in pre-synaptic PIP_2 concentration (Micheva et al. 2003). This PIP_2 prebinds with synaptotagmin (Ca^{2+} sensor protein of the synaptic vesicles release machinery) and increases the

Table 8 List of parameters used for post-synaptic Ca^{2+} dynamics

Symbol	Description	Value	Reference
η	Fraction Ca^{2+} current carried by AMPAR	0.012	Bollman et al. 2000
P_{open}	VGCC open probability	0.52	Sabatini and Svoboda 2000
K_{endo}	Ca^{2+} affinity of Endogenous buffer	10 μM	Keller et al. 2008
b_{t}	Total endogenous buffer concentration	200 μM	See text, Page No. 19
V_{R}	Reversal potential of Ca^{2+} ion in spine	27.4 mV	Sochivko et al. 2002
V_{spine}	Volume of dendrite spine	0.9048 μm^3	See text, Page No. 17
$c_{\text{post}}^{\text{rest}}$	Resting post-synaptic Ca^{2+} concentration	100 nM	
k_{s}	Maximum PMCa efflux rate	100/s	Keller et al. 2008
g_{R}	Conductance of R-type channel	15 pS	Sabatini and Svoboda 2000
N	Number of R-type channels	12	Sabatini and Svoboda 2000

affinity of the synaptotagmin for the boutonic Ca^{2+} (Bai et al. 2004). This implies that increasing PIP_2 concentration enhances the rate with which Ca^{2+} binds to the pre-synaptic Ca^{2+}—sensor. The rate with which Ca^{2+} binds to pre-synaptic Ca^{2+}—sensor is given by Ca^{2+} association rate constant (α) (see equation (6)). α has been modeled to depend directly on phosphorylated CaM-KII concentration (due to the lack of exact mechanism by which CaM-KII affects PIP_2 via NO, and consequently the rate with which Ca^{2+} binds with pre-synaptic Ca^{2+}—sensor).

We have used the mathematical model of CaM-KII phosphorylation due to Zhabotinsky (2000). The model consists of 10 subunits. When two neighboring subunits bind with $(Ca^{2+})_3$CaM (where the subscript denotes 3 Ca^{2+} ions), the first one phosphorylates the second one in clockwise direction. This initial step can be summarized by the following reactions

$$3Ca^{2+} + CaM \rightleftharpoons C, \tag{28}$$

$$P_0 + C \rightleftharpoons P_0C, \tag{29}$$

$$P_0C + C \rightleftharpoons P_0C_2, \tag{30}$$

$$P_0C_2 \xrightarrow{K_1} P_1C_2. \tag{31}$$

Here C denotes Ca^{2+} bound with calmodulin, P_0 is the unphosphorylated CaM-KII holoenzyme, P_1 is the one-fold phosphorylated CaM-KII holoenzyme. The rate of the initiation step or the rate of the phosphorylation is

$$v_{\text{phos}} = 10K_1P_0\frac{\left(c_{\text{post}}^{n_{h_1}}\right)^2}{\left(k_{h_1}^{n_{h_1}} + c_{\text{post}}^{n_{h_1}}\right)^2}, \tag{32}$$

where K_1 is the rate at which P_0C_2 is phosphorylated (see equation (31)), 10 is the statistical factor, k_{h_1} is the post-synaptic Ca^{2+} concentration at which v_{phos} is halved and n_{h_1} is the Hill coefficient for the rate of phosphorylation. Further, Zhabotinsky (2000) assumed that catalytic activity of the autophosphorylated subunit does not depend on the binding of C and in this case the rate of autophosphorylation can be given by the following reactions

$$P_1 + C \rightleftharpoons P_1C, \tag{33}$$

$$P_1C \xrightarrow{K_1} P_2. \tag{34}$$

Correspondingly the per-subunit rate of autophosphorylation is

$$v_{\text{a-phos}} = K_1\frac{c_{\text{post}}^{n_{h_1}}}{k_{h_1}^{n_{h_1}} + c_{\text{post}}^{n_{h_1}}}. \tag{35}$$

Here, K_1 is the rate constant of equation (34) which is the same as of equation (31). Dephosphorylation of subunits proceeds according to the following MM scheme

$$SP + E \rightleftharpoons SPE \longrightarrow E + S. \tag{36}$$

Here S is an unphosphorylated subunit, SP is a phosphorylated subunit, E is a protein phosphatase and SPE is the phosphorylated subunit bound with protein phosphatase. Following Zhabotinsky (2000) the per-subunit rate of dephosphoryaltion is

$$v_{\text{d-phos}} = \frac{K_2e_{\text{p}}}{K_{\text{M}} + \sum_1^{10} iP_{\text{i}}}, \tag{37}$$

where e_{p} is the concentration of active protein phosphatase, and K_2 and K_{M} are catalytic and MM constants, respectively. Four protein phosphotases dephosphorylate CaM-KII: PP1, PP2A, PP2C and a specific CaM-KII phosphatase (Zhabotinsky 2000). PP1 is the only protein which dephosphorylates CaM-KII in PSD (Zhabotinsky 2000). Activity of PP1 can be controlled by Ca^{2+}/CaM via inhibitor 1 (I1), calcineurin (CaN) and protein kinase A (PKA). PKA

phosphorylates I1 and CaN dephophorylates it (see Fig. 2). Although, phosphorylated form of the inhibitor-1 (I1P) is known as a potent inhibitor of PP1 (by forming a complex PP1–I1P, which inactives the PP1 activity) (Zhabotinsky 2000); its de-phosphorylated form is known to stimulate the PP1 activity (Munton et al. 2004).

Hence a modification was made to the equation governing PP1 concentration in Zhabotinsky (2000) to incorporate the I1 dependent PP1 production (see broken line Fig. 2). Also recent values of PKA based phosphorylation of I1 were used (Sahin et al. 2006). The mathematical model governing CaM-KII phosphorylation can be given by the following equations (Lisman and Zhabotinsky 2001)

$$\begin{aligned}
\frac{dP_0}{dt} &= -v_{\text{phos}} + v_{\text{d-phos}} P_1 \\
\frac{dP_1}{dt} &= v_{\text{phos}} - v_{\text{d-phos}} P_1 - v_{\text{a-phos}} P_1 + 2v_{\text{d-phos}} P_2 \\
\frac{dP_i}{dt} &= v_{\text{a-phos}} w_{i-1} P_{i-1} - v_{\text{d-phos}} i P_i - v_{\text{a-phos}} w_i P_i + v_{\text{d-phos}} (i+1) P_{i+1} \\
\frac{dP_{10}}{dt} &= v_{\text{a-phos}} P_9 - v_{\text{d-phos}} 10 P_{10} \\
\frac{de_p}{dt} &= -k_F I e_p + k_B (e_{p0} - e_p) + k_I I_0 \\
\frac{dI}{dt} &= -k_F I e_p + k_B (e_{p0} - e_p) + v_{PKA} \frac{I_0}{I_0 + K_{PKA}} - v_{CaN} I \frac{c_{post}^3}{k_{h_2}^3 + c_{post}^3}
\end{aligned} \tag{38}$$

Here P_i is the i-fold phosphorylated CaM-KII holoenzyme, e_p is the concentration of PP1 not bound to I1P, e_{p0} is the total concentration of PP1, I is the concentration of free I1P and I_0 is the concentration of free I1. If 'i' subunits are phosphorylated then the effective number of subunits capable of autophosphorylating are $w_2=w_8=1.8$, $w_3=w_7=2.3$, $w_4=w_6=2.7$, $w_5=2.8$ (here subscript is 'i'). k_F and k_B are respectively the association and dissociation rate constant of PP1–I1P complex. k_{h_2} is the Hill constant of CaN dependent dephosphorylation of I1P, v_{CaN} is the rate of dephosphorylation of I1P due to CaN, K_{PKA} is the MM constant of PKA, v_{PKA} is the rate of phosphorylation of I1 by PKA, k_I is an experimentally undetermined rate, with which I1 regulates PP1 activity, fixed with the help of computer simulations. The importance of incorporating I1 dependent PP1 production is that the CaM-KII phosphorylation process becomes reversible, rather than bi-stable (having two stable steady-states), as found experimentally by Bradshaw et al. (2003). The value of the parameters is listed in Table 9. For more details on the model see Zhabotinsky (2000).

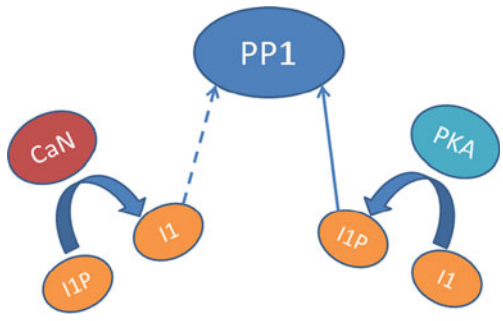

Fig. 2 Schematic representation of PP1 activity regulation by CaN and PKA. CaN dephosphorylates I1P and promotes PP1 activity via I1 (*broken line*). PKA phosphorylates I1 and inhibits PP1 activity via I1P (*solid line*)

As explained earlier, it is assumed that the phosphorylated CaM-KII stimulates NO production. Produced NO is free to diffuse to the pre-synaptic terminal, where it enhances the rate with which Ca^{2+} binds with the synaptic vesicle Ca^{2+}—sensor. Mathematically this has been achieved by increasing the rate with which Ca^{2+} binds with Ca^{2+}—sensor (synaptotagmin) i.e. increasing the value of Ca^{2+} association rate (α) with Ca^{2+}—sensor. The percent increase in the Ca^{2+} association rate (α) is an important parameter and has been termed as k_{syt}. Only a small increment of 5 % in α value could yield us a persistent increase, up to 80 %, in synaptic efficacy. The increase in α value is governed by a sigmoidal function given by

$$\frac{k_{syt}}{1 + \exp\left(-\frac{\left(\left(\sum_1^{10} P_i\right) - P_{1/2}\right)}{k_{1/2}}\right)}. \tag{39}$$

Here $P_{1/2}$ is the (choosen to be half of the total CaM-KII concentration inside PSD) threshold value of phosphorylated CaM-KII after which it stimulates NO production, $k_{1/2}$ is the slope giving the increment a switch like behavior which is dependent upon the phosphorylated CaM-KII concentration. It is apparent from equation (39) that the increment can achieve a maximum of k_{syt} for a fully phosphorylated CaM-KII. We simulated the model for varying values of k_{syt} and demonstrated the change in LTP for pre-astrocytic to post-astrocytic activities. The value of the parameters is appended in Table 9.

2.11 Numerical implementation

All the computations and visualizations of the model are implemented in MATLAB environment. The model equations were discretized with a temporal precision of, $\Delta t = 0.05$ ms. The canonical explicit Euler method was used to solve the system of thirty-six ordinary differential equations governing TpS. For the numerical simulation of the noise term, in equation (12), we have used Box-Muller Algorithm (Fox 1997) to generate the noise-term at each time-step (Δt). All simulations were performed on a Dell Precision T3500 workstation with Intel Xeon processor (4 parallel CPUs) with 2.8 GHz processing speed and with 12 GB RAM. Simulating real time of 1 min takes approximately 9.5 min of simulation time. The MATLAB script written for the

Table 9 List of parameters used for CaM-KII Phosphorylation

Symbol	Description	Value	Reference
k_F	Association rate constant of PP1—I1P complex	1/μM s	Zhabotinsky 2000
k_B	Dissociation rate constant of PP1—I1P complex	10^{-3}/s	Zhabotinsky 2000
k_I	I1 dependent regulation rate of PP1	1/s	See text, Page No. 24
e_{p0}	Total concentration of PP1	0.1 μM	Zhabotinsky 2000
v_{PKA}	Phosphorylation rate of I1 due to PKA	0.45 μM/s	Sahin et al. 2006
K_{PKA}	MM constant of I1 phosphorylation rate	0.0059 μM	Sahin et al. 2006
v_{CaN}	Rate of I1P dephosphorylation due to CaN	2/s	Lisman and Zhabotinsky 2001
k_{h_2}	Ca^{2+} activation Hill constant of CaN	0.7 μM	Zhabotinsky 2000
K_1	Catalytic constant of autophosphorylation	0.5/s	Zhabotinsky 2000
k_{h_1}	Ca^{2+} activation Hill constant of CaM-KII	4.0 μM	Zhabotinsky 2000
n_{h_1}	Hill coefficient for Ca^{2+} activation of CaM-KII	3	Miller et al. 2005
K_2	Catalytic constant of PP1	10/s	Bradshaw et al. 2003; Miller et al. 2005
K_M	MM constant of PP1	20 μM	Zhabotinsky 2000
I_0	Concentration of free I1	0.1 μM	Zhabotinsky 2000
k_{syt}	Percent increase in Ca^{2+} association rate of synaptotagmin	0.5 %	See text; Page No. 25
$P_{1/2}$	Threshold for phosphorylated CaM-KII based NO production	40 μM	See text; Page No. 26
$k_{1/2}$	Slope factor for activation of CaM-KII based NO production	0.4 μM	See text; Page No. 26
e_k	Total CaM-KII concentration in PSD	80 μM	Zhabotinsky 2000

simulation of the model is supplied with the Supporting Material.

3 Simulation results

3.1 Astrocyte-independent information processing

We first demonstrate how the model would behave in an astrocyte-independent pathway (see Fig. 1). The results are shown for a typical simulation elicited in response to a stimulus current of density 10 μA cm^{-2} (frequency 5 Hz, duration 10 ms), imitating the single pulses stimulus used by Perea and Araque (2007) in their experiments. The experiments performed by Perea and Araque (2007) were considering an open loop i.e. simultaneous stimulation of SC and astrocyte. Such parallel stimulation of SC and astrocyte can occur at a TpS under physiological condition. But the pharamacological stimulus of astrocyte used in their experiments may or may not e.g., UV-flash stimulated NP-EGTA mediated Ca^{2+} uncaging in astrocytes at first appears to be an excellent approach to study Ca^{2+}—dependent processes. However there are caveats associated with this approach (Agulhon et al. 2008). Thus in our model we have considered a closed loop, where astrocyte is excited in an activity-dependent manner i.e. astrocytic Ca^{2+} rises in response to the glutamate released in the cleft from SC.

Asking the question of the effect of an astrocyte over the synaptic plasticity, Perea and Araque (2007) first only stimulated the SC and not the astrocyte. The present section is analogous to their experimental setup studying synaptic efficacy, synaptic potency and Pr in absence of astrocyte. In Fig. 2, important components like pre-synaptic membrane potential, bouton Ca^{2+} concentration, synaptic glutamate and post-synaptic membrane potential are shown. The model was simulated for a duration of 30 min. But the results in Fig. 3 have been shown for 60 s just for the sake of clarity of the involved variable.

To simulate the astrocyte-independent information flow from the pre-synaptic bouton to the post-synaptic spine, we clamped astrocyte Ca^{2+} to its resting value regardless of the stimulus (in the form of released synaptic glutamate) received at astrocytic mGluR. Figure 3(a) is the pre-synaptic AP generated at the axon-hillock in response to the current injected at soma. As assumed, AP propagates without degradation to the axon bouton leading to the opening of the VGCCs. The Ca^{2+} current carried by the VGCC leads to an increase in the bouton Ca^{2+} concentration (see Fig. 3(b)). The Ca^{2+} inside the bouton is generally released in close proximity of the synaptic vesicles which binds with its Ca^{2+}—sensor instigating the process of exocytosis (see Fig. 3(c)). The released glutamate is free to diffuse and binds with glutamate receptors (AMPAR on the post-synaptic spine and mGluR on the astrocyte surface). Since astrocyte Ca^{2+} was clamped to its resting concentration there is no amplification of the information (see Fig. 1)

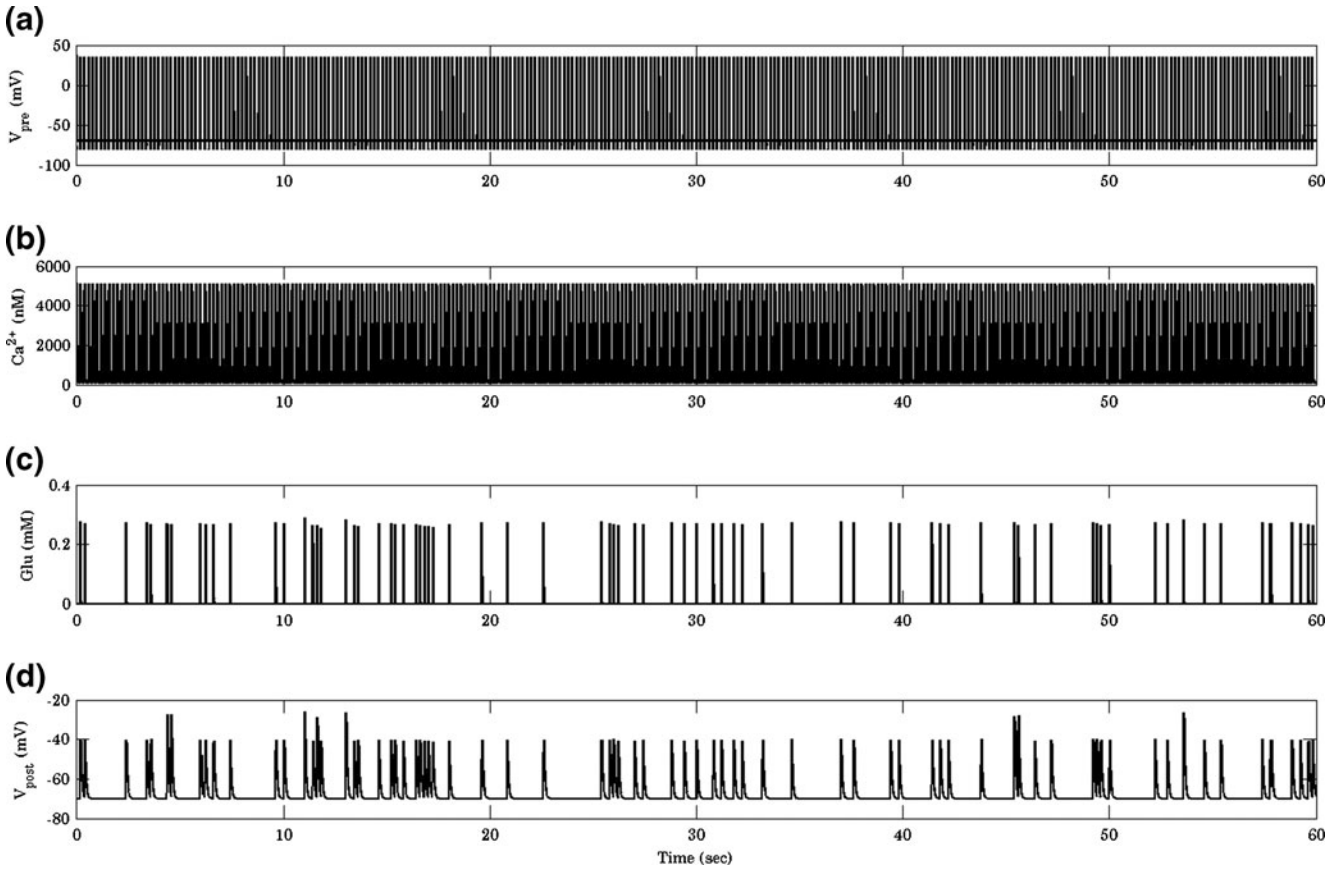

Fig. 3 Components involved in astrocyte-independent pathway of information processing. (**a**) Pre-synaptic AP, generated at axon-hillock in response to the stimulus. (**b**) Ca^{2+}, as a result of AP invading axon boutons. (**c**) Glutamate, released in the synaptic cleft due to exocytosis of vesicles in a Ca^{2+}—dependent manner. (**d**) Excitatory Post-Synaptic Potential (EPSP), due to opening of ionotropic glutamate receptors (here, AMPARs) on the surface of spine-head

due to it and hence omitted. Glutamate bound with AMPARs causes depolarization of post-synaptic membrane (see Fig. 3(d)). Figure 3(d) basically reflects the transduction of the input signal (see Fig. 3(a)). It should be noted that the given process of signal transduction does not make any contribution due to the astrocyte-dependent pathway. The synaptic strength for the present synapse is calculated in a way analogous to Perea and Araque (2007). We calculated synaptic efficacy (windowed-mean of post-synaptic responses including success and failures), synaptic potency (windowed-mean of successful post-synaptic responses) and Pr (given as a measure of signal transduction i.e. ratio of the input pulse being converted into the output response). Data are expressed as mean±standard deviation. The results were compared using a two-tailed Student's *t*-test. Statistical significance is established with $P<0.01$.

It is apparent from Fig. 4 that the synaptic efficacy remains unchanged prior to post– synaptic neuron depolarization (to –30 mV) and after 10 min of post-synaptic depolarization (before: 0.029±0.005 pA; after 10 min: 0.028±0.005 pA; $P=0.51$). Similarly, probability of neurotransmitter release Pr remained unchanged prior to the post-synaptic depolarization and 10 min after post–synaptic depolarization (before: 0.26±0.05; after 10 min: 0.25±0.05; $P=0.53$). Synaptic potency also remained unperturbed (before: 4.27±0.07 pA; after 10 min: 4.26±0.07 pA; $P=0.71$) prior to post-synaptic depolarization and 10 min after post-synaptic depolariztion. Our observations are in agreement with the experimental observations of Perea and Araque (2007), when peri-syanptic astrocyte was not photo-simulated, which validates our model at an astrocyte-independent synapse.

In Fig. 5(a), we show post-synaptic spine Ca^{2+} concentration due to the fractional current carried by AMPARs and VGCCs. Also, one can see a cluster of Ca^{2+} peaks at the 10 min mark, which is in response to post-synaptic membrane depolarization to –30 mV. Whenever post-synaptic membrane is depolarized (for more than –30 mV) they lead to opening of VGCCs (depending upon $B(N,P_{open})$, see equation (25)) located at the spine. VGCCs are responsible for the cluster of Ca^{2+} peaks visible in Fig. 5(a). Inflow of excess Ca^{2+} through VGCCs is good enough to phosphorylate CaM-KII above the threshold ($P_{1/2}$), see Fig. 5(b). The transient increase in Pr, visible in Fig. 4(b), is as a result of

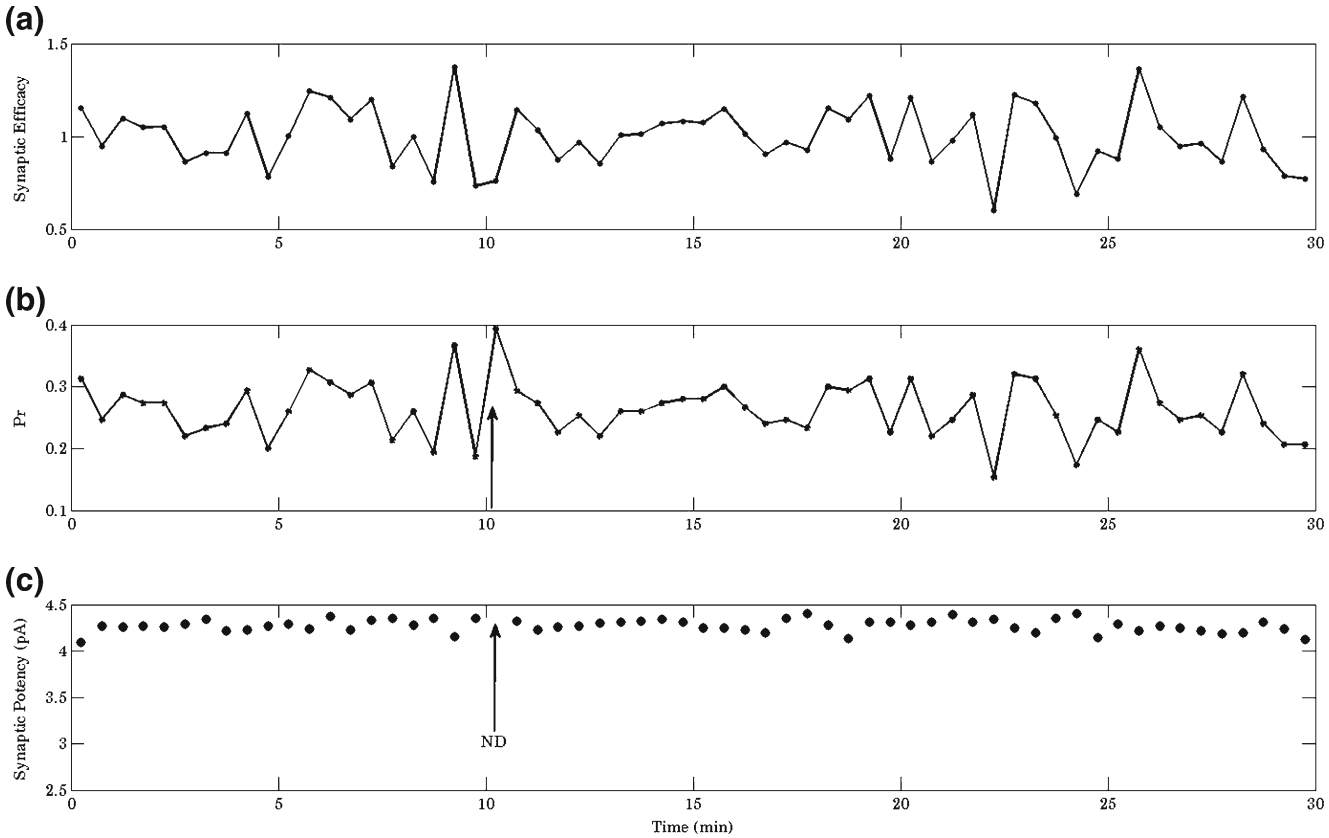

Fig. 4 Synaptic parameters given as synaptic efficacy, probability of neurotransmitter release and synaptic potency. The black arrow (↑) is to show the time at which post-synaptic neuron was depolarized to -30 mV; ND: Neuronal Depolarization. (**a**) Synaptic efficacy, (**b**) Probability of neurotransmitter release and c. Synaptic potency has been averaged over a time–window of 30 s

CaM-KII crossing the threshold (see Fig. 5(b)). However, in absence of astrocyte the frequency of the post-synaptic Ca^{2+} response is not strong enough to keep it phosphorylated above $P_{1/2}$. Consequently, CaM-KII is de-phosphorylated below the threshold and Pr comes down to values prior to the post-synaptic depolarization.

Figure 6 displays the evolution of the variables involved in CaM-KII phosphorylation process see equation (38). First we show the evolution of 0-fold phosphorylated CaM-KII holoenzyme, P_0 in equation (38), which is equal to the total CaM-KII concentration (e_k) minus phosphorylated CaM-KII concentration (i.e. equal to the sum of all i-fold phosphorylated CaM-KII holoenzymes or $\sum_{i=1}^{10} P_i$) shown in Fig. 5(b). It is interesting to note that, here, CaM-KII dephosphorylation process follows the scheme shown in equation (36). The relationship between 0-fold phosphorylated CaM-KII (or unphosphorylated CaM-KII) and phosphorylated CaM-KII is straightforward i.e. $P_0 = e_k - \sum_{i=1}^{10} P_i$. It is solely because in PSD CaM-KII concentration is much more than PP1 concentration, because of which the amount of CaM-KII bound with PP1 is negligible compared to the total CaM-KII concentration. This condition is also a reason behind the choice of MM kinetics for CaM-KII dephosphorylation process by Zhabotinsky (2000). PP1 (see Fig. 6(c)) is deactivated by phosphorylated I1 (see Fig. 6(b)). When I1P concentration is the lowest then PP1 concentration is the highest (at the 10 min mark). In Fig. 6(c) we can see a sharp spike in PP1 concentration which is due to a rapid fall in I1P concentration contributed by CaN via the cluster of Ca^{2+} peaks (see Fig. 5 (a)). Evolution of all i-fold phosphorylated CaM-KII holoenzymes (P_i) is provided with the supplementary material.

3.2 Astrocyte-dependent information processing

We went ahead and investigated if clamping and unclamping of astrocytic Ca^{2+} concentration would yield modifications similar to Perea and Araque (2007). They stimulated SC and astrocyte simultaneously to study the astrocytic role in synaptic strength modulation i.e. considering an open loop. However we considered a closed loop where astrocytic Ca^{2+} is modulated by pre-synaptically released glutamate (Porter and McCarthy 1996) which in turn modulates pre-synaptic Ca^{2+} in a mGluR-dependent pathway (Fiacco and McCarthy 2004; Perea and Araque 2007). To validate the fact that astrocytes modulate synaptic strength via an mGluR-dependent pathway Perea and Araque (2007)

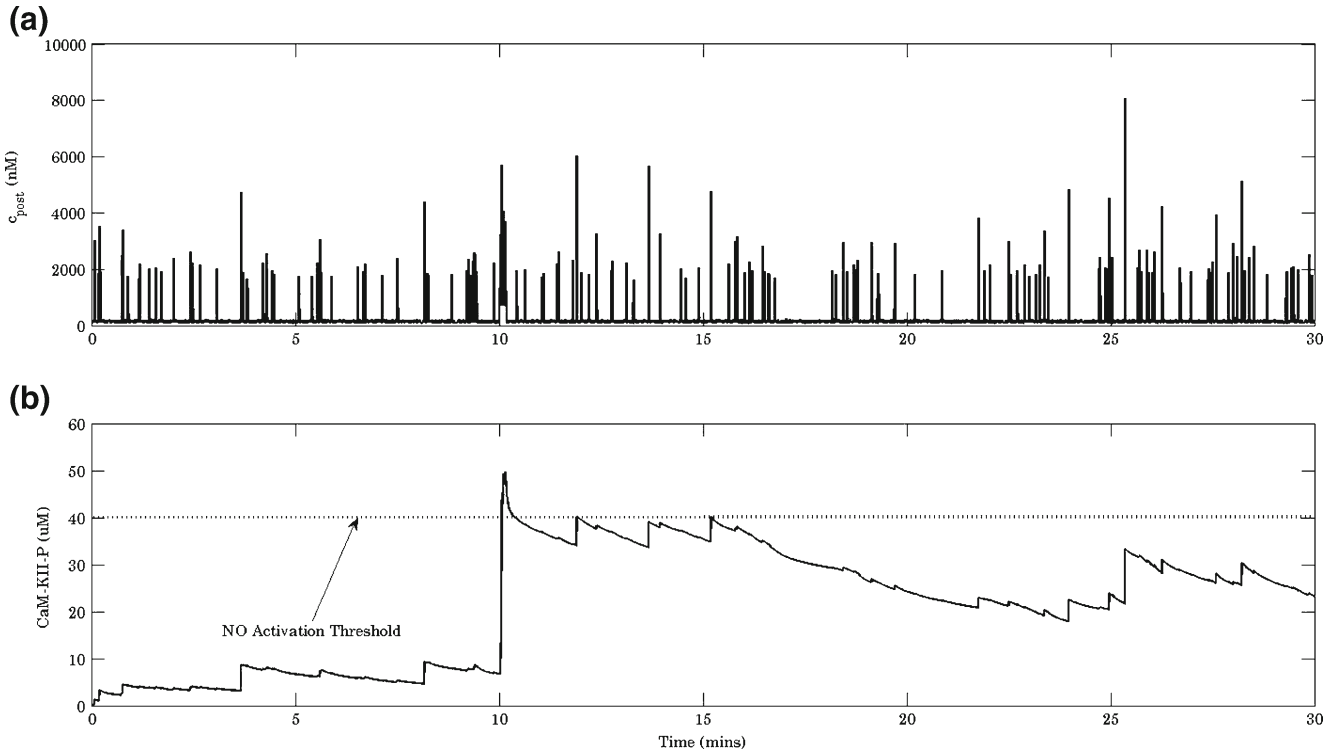

Fig. 5 Post-synaptic variables responsible for stimulating NO production in our model. (**a**) Post-synaptic spine Ca^{2+} concentration. (**b**) Phosphorylated CaM-KII (CaM-KII-P) concentration. Note the sudden spike in phosphorylated CaM-KII concentration at 10 min which is in response to mild-depolarization of post-synaptic neuron to –30 mV for duration of 10 s

continuously stimulated SC and evoked astrocytic Ca^{2+} responses, using UV-flash via NP-EGTA, to find a transient enhancement of synaptic efficacy when astrocyte was photo-stimulated. Similar to their experimental approach we kept astrocytic Ca^{2+} concentration clamped for the first 10 min imitating the behavior of NP-EGTA in their experiments. The astrocyte Ca^{2+} clamping is turned off after 10 min. At the same time post-synaptic membrane is also depolarized to –30 mV.

In Fig. 7 we observe the changes in the model following an astrocyte-dependent approach of information processing. The release of Ca^{2+} from bouton stores (ER) contributes to the transient increase in $[Ca^{2+}]$ (which is held responsible for modulating spontaneous transmitter release—Emptage et al. (2001)). With the information flow following an astrocyte-dependent approach, it is assumed that the agonist (glutamate, necessary for Ca^{2+} release from ER), which causes cleavage (in a G-protein dependent manner) of PIP_2 into IP_3 and DAG, comes from the peri-synaptic astrocyte. Here we can observe that there is no change in bouton IP_3 concentration till it reaches 10 min mark (see Fig. 7a). It is because of an assumed clamping of astrocytic Ca^{2+} by NP–EGTA.

As soon as we remove the astrocytic Ca^{2+} clamp, we can see an increase in IP_3 concentration, which opens the IP_3R on the surface of ER. Further flow of Ca^{2+} ions inside bouton cytosol due to release of Ca^{2+} from ER elevates the averaged Ca^{2+} concentration (see Fig. 9a). Ca^{2+} binds with Ca^{2+}—sensor of the vesicles and instigates exocytosis of synaptic vesicles filled with glutamate (see Fig. 7c). In a process similar to the one defined earlier, the synaptic glutamate leads to production of IP_3 but this time inside the astrocyte. Produced IP_3 binds with the IP_3R which sets up inflow of Ca^{2+} from the ER into the astrocytic cytosol (see Fig. 7e). Astrocytic Ca^{2+} binds with its Ca^{2+}—sensor synaptotagmin IV protein (Montana et al. 2006) to initiate exocytosis of the SLMV's content (glutamate) in the extra-synaptic cleft (see Fig. 7e). This spilled extra-synaptic glutamate is the necessary "agonist" mentioned in the earlier paragraph, which is responsible for the fluctuations of the bouton IP_3 (see Fig. 7a) setting up enhanced bouton Ca^{2+} concentration (see Figs. 7b and 8).

The effect of astrocyte-dependent pathway over the bouton Ca^{2+} is pretty evident in Fig. 7, but if this increase is playing any role at all in modulating the synaptic parameters, we that's what investigated next. We calculated synaptic efficacy, probability of neurotransmitter release and synaptic potency, as defined previously, using a time-window of length 30 s. We again made use of two-tailed student's *t*-test and established statistical significance (with $P<0.01$) as defined earlier. The statistical inference did support the fact that astrocytes modulate synaptic

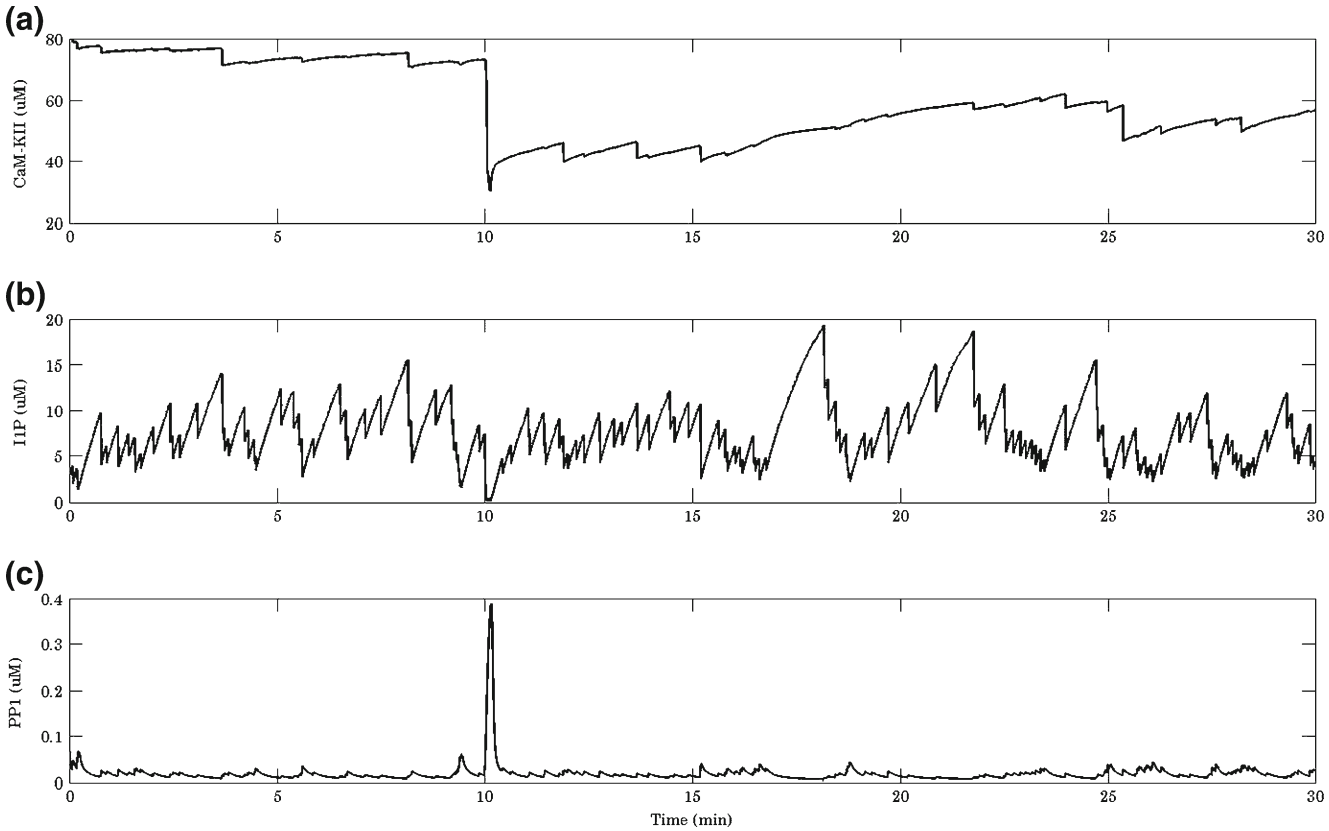

Fig. 6 Some important variables involved in CaM-KII phosphorylation. (**a**) 0-fold phosphorylated CaM-KII concentration, (**b**) Phosphorylated I1 concentration, C. Free PP1 concentration (not bound to I1P)

parameters. The synaptic efficacy exhibited a persistent (≥20 min) LTP of up to 180 % after mild post-synaptic neuron depolarization and astrocytic Ca^{2+} unblock (from 0.028±0.003 pA to 0.038±0.004 pA ($P<0.001$), before and 10 min after the astrocyte stimulation, respectively). In the experiments of Perea and Araque (2007) the locus of LTP induction was purely pre-synaptic, which was confirmed with the two tailed *t*-test of persistently unchanged synaptic potency. Similar to them we also performed a two tailed *t*-test on the averaged synaptic potency prior to the post-synaptic depolarization and 10 min after the post-synaptic depolarization. There was no statistically significant change in synaptic potency after LTP induction (4.25± 0.07 pA and 4.23±0.07 pA, before and 10 min after the astrocytic stimulation; $P=0.43$) validating the pre-synaptic locus of induction.

Next we checked if the persistent increase in probability of neurotransmitter release is associated with this form of LTP. Indeed we found a persistent increase in Pr (from 0.25 ±0.03 to 0.35±0.04; $P<0.001$), before and 10 min after the astrocyte stimulation. This persistent increase in probability is due to an enhanced bouton average Ca^{2+} concentration, visible after astrocyte Ca^{2+} unblock (see Fig. 9a). Another important reason related with this persistent probability increase is the mild post-synaptic depolarization to –30 mV. The depolarization of post-synaptic membrane to –30 mV causes VGCCs located at the spine to open, which brings additional Ca^{2+} (apart from the fraction of Ca^{2+} carried by AMPARs) inside the spine (see Fig. 10a for a cluster of Ca^{2+} peaks). This cluster of Ca^{2+} peaks (at the 10 min mark), instigated by the post-synaptic depolarization, plays an important role in phosphorylating CaM-KII above the threshold (see Fig. 10b) and stimulates NO production (as explained in subsection 2.10). We followed the similar procedure to stimulate NO production in astrocyte-independent pathway of information processing, but in vain, as frequency of post-synaptic spine [Ca^{2+}] was unable to keep CaM-KII phosphorylated. However it is apparent from Fig. 10b that in an astrocyte-dependent pathway a similar post-synaptic depolarization leads to a persistent increase in Pr and consequently, a persistent increase in synaptic efficacy, termed as LTP. It should be pointed out that in both the cases post-synaptic membrane was depolarized (to –30 mV) for a duration of 10 s. The opening of VGCCs was governed by a BRN therefore a similar stimulus will open different number of VGCCs each time. Therefore for the sake of a fair comparison between the two pathways (astrocyte-dependent and astrocyte-independent) we ran simulations so that CaM-KII is phosphorylated (above the threshold for NO production) to the same extent for both pathways (as it will be

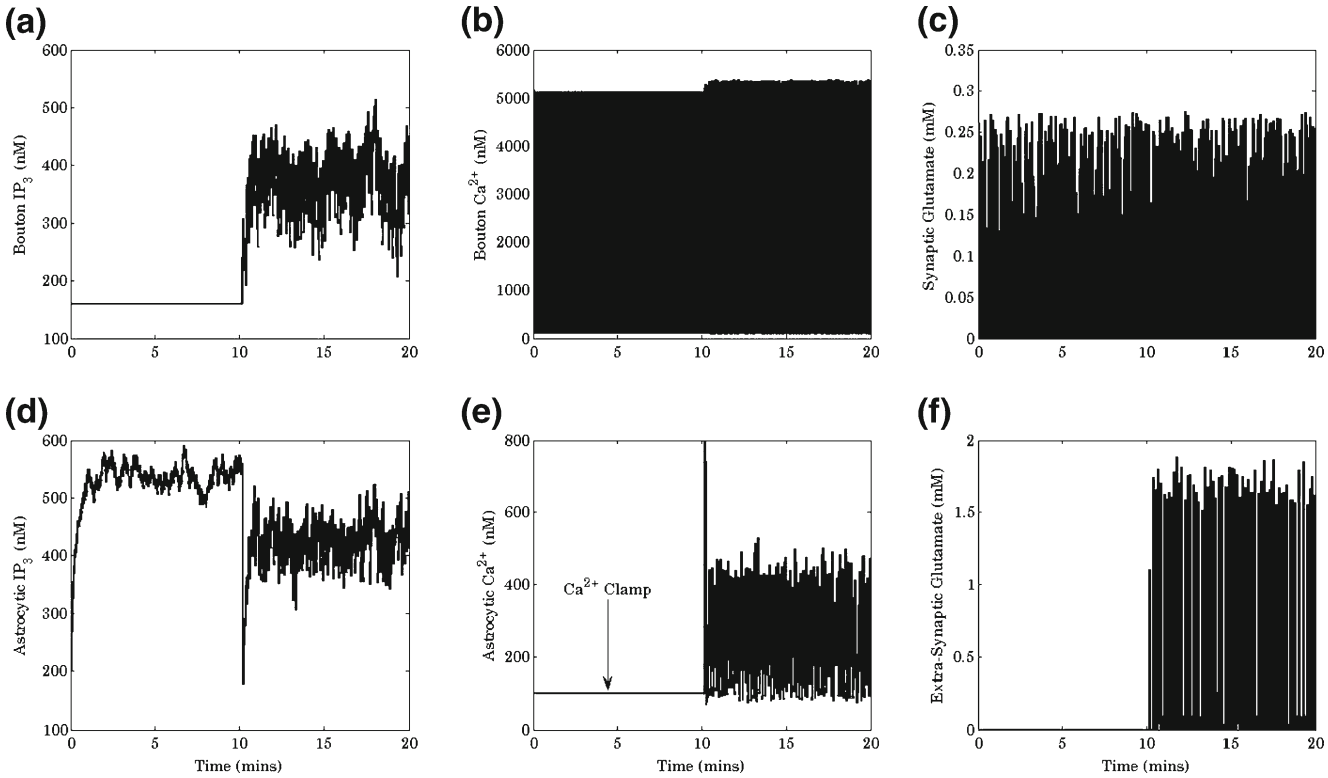

Fig. 7 Components involved in astrocyte-dependent information processing. (**a**) Bouton IP_3, (**b**) Bouton Ca^{2+} averaged in a time-window of length 30 s, (**c**) Synaptic Glutamate, in response to exocytosis of synaptic vesicles, (**d**). Astrocytic IP_3, due to synaptic glutamate binding with mGluRs on the surface of astrocyte, (**e**). Astrocyte Ca^{2+}, elicited in response to Ca^{2+} released from ER, (**f**). Extra-synaptic glutamate, due to a possible exocytosis of SLMVs

evident from Figs. 5b and 10b. It is≈50 μM in both the cases). It should also be stated that the difference between the two-pathways remained apparent regardless of the extent to which CaM-KII is phosphorylated in response to a post-synaptic membrane depolarization. However it did modify the time with which CaM-KII decays below $P_{1/2}$ with stronger depolarization increasing time required for CaM-KII, to decay below $P_{1/2}$.

In any case, when CaM-KII decays below $P_{1/2}$ under astrocyte-independent pathway it stays below it (see Fig. 5b). However even if it goes below $P_{1/2}$ following astrocyte-dependent pathway it again goes above $P_{1/2}$ (see Fig. 10b), because of more frequent post-synaptic Ca^{2+} responses due to enhanced average bouton Ca^{2+} concentration (see Fig. 9a). There was a clear distinction in CaM-KII phosphorylation process when astocyte was and wasn't photo-stimulated. Even the extent to which CaM-KII is phosphorylated was quite evident and $P_{1/2}$ could be fixed accordingly to predict the threshold for NO production (tested for K_M (M–M constant of PP1 dependent dephosphorylation of CaM-KII) values of 2.5 μM, 5 μM, and 10 μM while keeping all other parameters fixed (see Fig. 11)). It can be observed from Fig. 11, that the threshold value of NO production ($P_{1/2}$) can always be fixed to be twice the MM constant of PP1 (K_M) dependent dephosphorylation of CaM-KII. The threshold of NO production basically defines the extent to which CaM-KII can be phosphorylated in an astrocyte-independent pathway of information processing (see the dotted line in Fig. 11).

In Fig. 12 we show some important variables associated with CaM-KII phosphorylation process performed mathematically using equation (38). As explained earlier the relationship between 0-fold phosphorylated CaM-KII and phosphorylated CaM-KII is straightforward. It can also be observed from Fig. 12a that it is very similar to Fig. 10b however inverted. PP1 (see Fig. 12c) is deactivated by I1P (see Fig. 12b). Following Zhabotinsky we assumed the concentration of free I1 as constant (at 0.1 μM). But one can observe from Fig. 12b (and likewise from Fig. 6b) that the concentration of phosphorylated I1 i.e. I1P is well above the free I1 concentration of 0.1 μM. Actually, the total concentration of I1 in PSD is significantly greater than free I1 (Miller et al. 2005) which is the case in our simulations. Evolution of all i-fold phosphorylated CaM-KII holoenzymes (P_i) is provided with the supplementary material.

The results discussed till now help establish our mathematical model, governing signal transduction, with and without the aid of a peri-synaptic astrocyte. A possible role

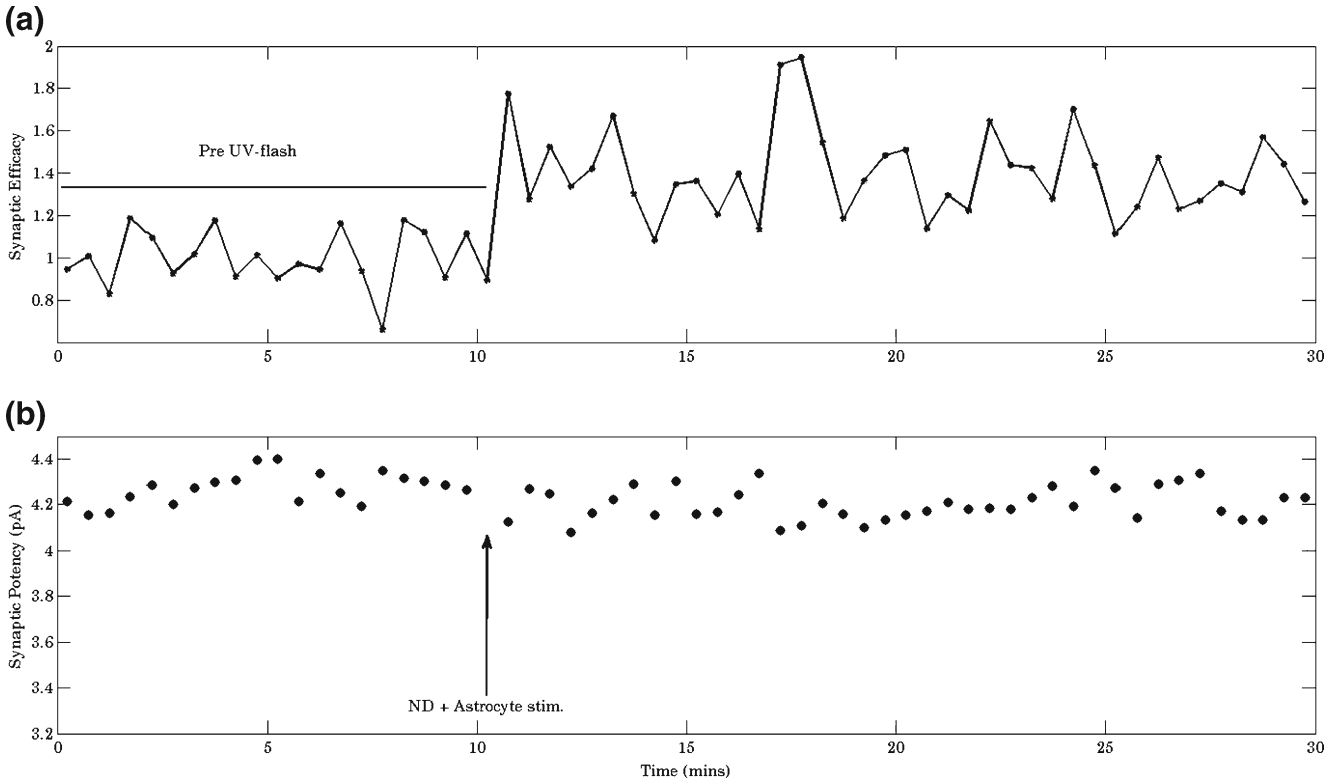

Fig. 8 Synaptic parameters namely, synaptic efficacy and synaptic potency given as a measure of synaptic plasticity in an astrocyte-dependent approach of information processing. (**a**) Synaptic efficacy is given by the average of EPSC amplitudes (including successes and failures) relative to the mean of EPSC amplitudes observed during the pre UV-flash period. Averages have been taken with a time-window of length 30 s, (**b**) Synaptic potency is given by the average of the successful post-synaptic responses using a time-window of length 30 s. The arrow (↑) indicates the time when astrocyte was switched on (Ca^{2+} unblock) and post-synaptic membrane was depolarized to –30 mV. ND=neuron depolarization

of astrocyte in LTP induction has been discussed and a mathematical framework under which it occurs is presented. However there are other important signaling cascades that can abolish LTP. One such important protein is I1 which deactivates PP1 and helps in LTP induction. A mice lacking I1 protein has been shown to have deficits in LTP induction (Bibb et al. 2001). Figure 13 demonstrates how such a mutation can abolish LTP in our model.

Mathematically we have achieved this by setting I_0=0 in equation (38). This results in $e_p = e_{p_0}$ and is equivalent to removing the last two equations in the equation (38) and treating e_p as a parameter. In Fig. 13 the value of e_p is equal to 0.05 μM. All other parameters are the same as listed in Tables 2, 3, 4, 5, 6, 7, 8 and 9. As expected removal of I1 from the PSD stops the I1 dependent deactivation of PP1 (which is responsible for dephosphorylating CaM-KII). Consequently PP1 continuously dephosphorylates CaM-KII (see Fig. 13a–b). In Fig. 13a we depolarized the post-synaptic membrane (to –30 mV) and observed the change in neurotransmitter release probability. There was no statistically significant change in Pr before ND and 10 min after it (before: 0.28±0.03; 10 min after: 0.26±0.04; P=0.15). We can observe from Fig. 13b, that even simultaneous stimulus of ND and astrocyte Ca^{2+} unblock could not keep CaM-KII-P above $P_{1/2}$ contrary to the behavior observed in Fig. 10b. However, we could observe a statistically significant change in Pr before stimulus (ND+astro. stim.) and 10 min after it (before: 0.26±0.04; 10 min after: 0.33±0.05; P<0.01). Indeed removal of I1 abolished LTP in our simulations but it could not abolish short-term potentiation (STP) due to transient increase in bouton Ca^{2+} concentration which is present only when astrocyte Ca^{2+} is unblocked (compare Fig. 13c and d). The transient enhancement in Pr can be observed in Fig. 13d, but not in Fig. 13c, which was also observed in the experiments of Perea and Araque (2007). Here we demonstrated that in our model LTP induction is abolished when I1 is removed similar to what has been observed experimentally (Bibb et al. 2001).

Using our computational model we could demonstrate that when ND is coupled with astrocyte stimulation a persistent increase in Pr can be observed. The increase in Pr observed in the experiments of Perea and Araque (2007) was nearly 2.5 times (before ND and astrocyte stimulation: 0.28±0.04; after ND and astrocyte stimulation: 0.71±0.08) while the increase observed in our model was nearly 1.5 times (before ND and astrocyte stimulation: 0.25±0.02;

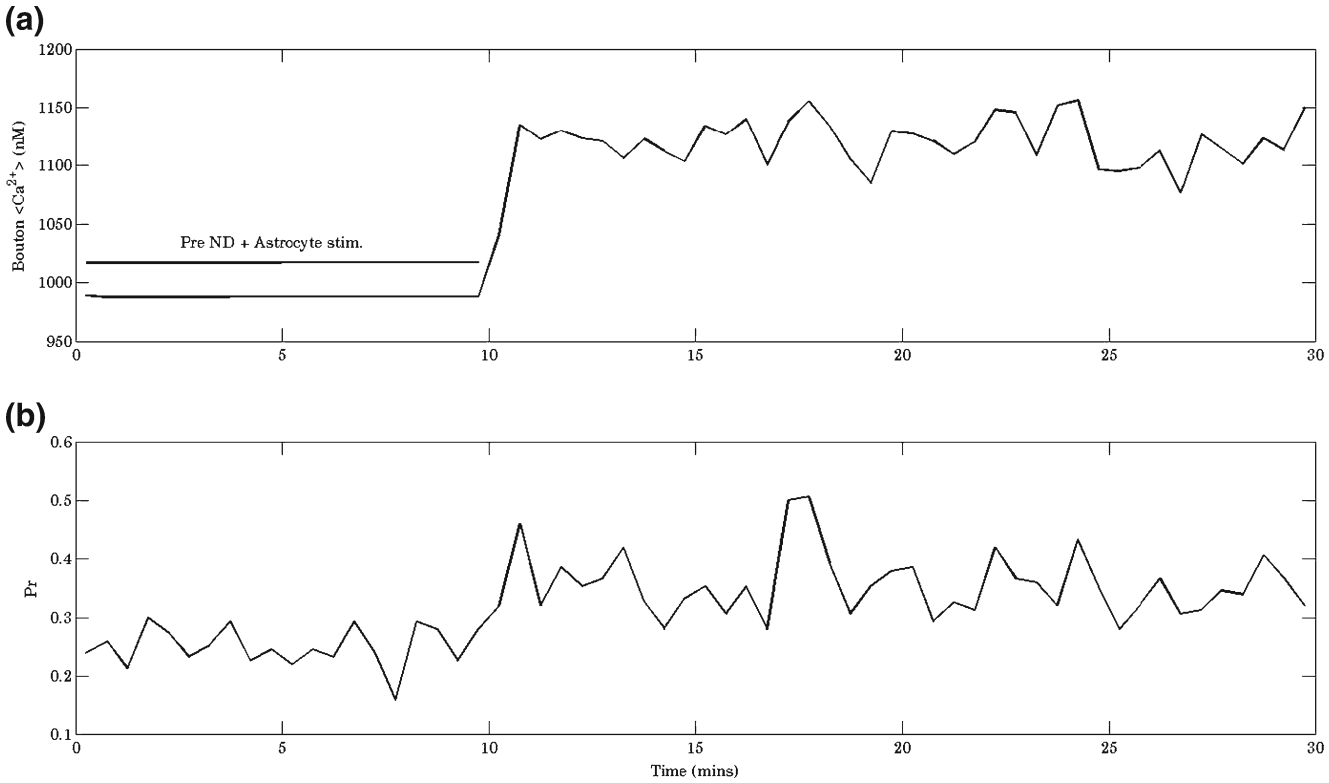

Fig. 9 (**a**) Averaged bouton Ca^{2+} concentration. (**b**) Probability of neurotransmitter release. The time-window for calculating the average was 30 s long in both the cases. Pre ND+astrocyte stim represents the phase prior to the post-synaptic membrane depolarization and astrocytic Ca^{2+} unblock

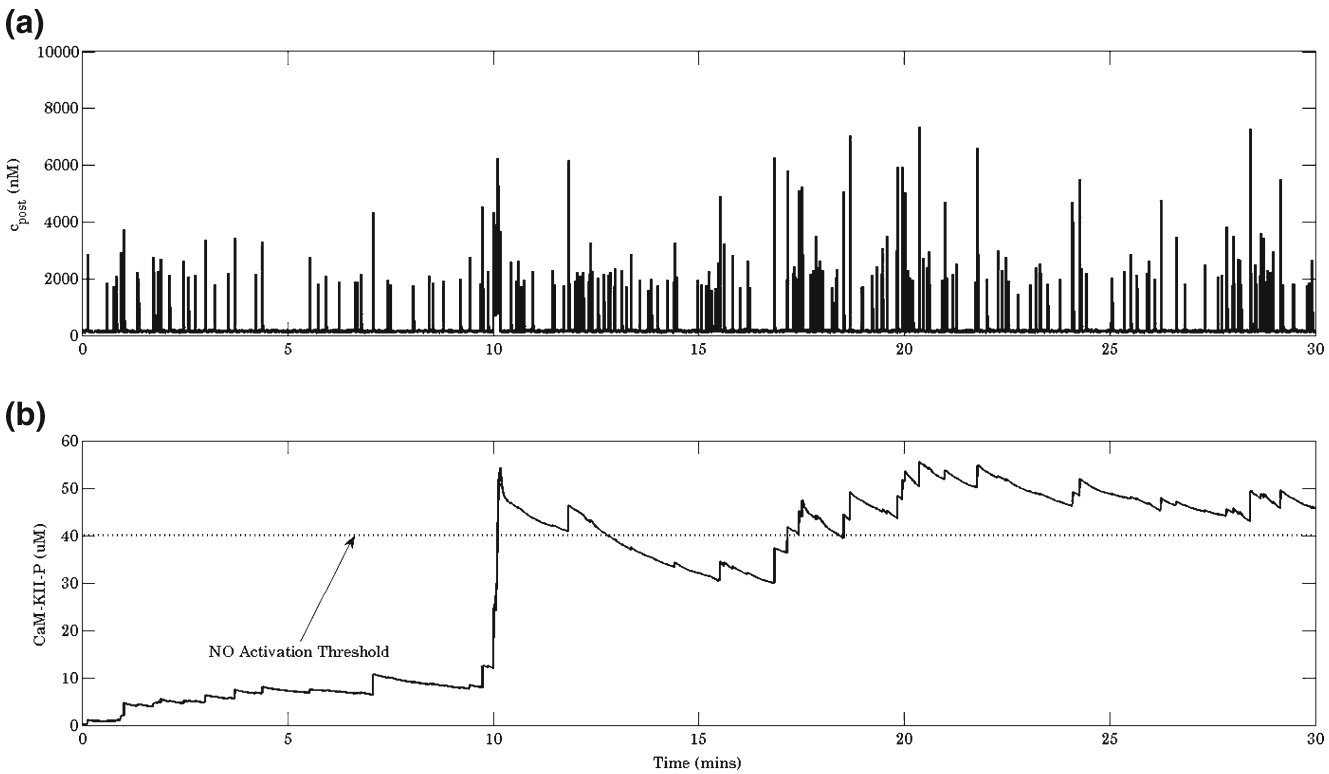

Fig. 10 Post-synaptic variables responsible for stimulating NO production in our model. (**a**) Post-synaptic spine Ca^{2+} concentration, (**b**) Phosphorylated CaM-KII (CaM-KII-P). The arrow (↑) points to the NO activation threshold, chosen to be the half of the total CaM-KII concentration inside PSD

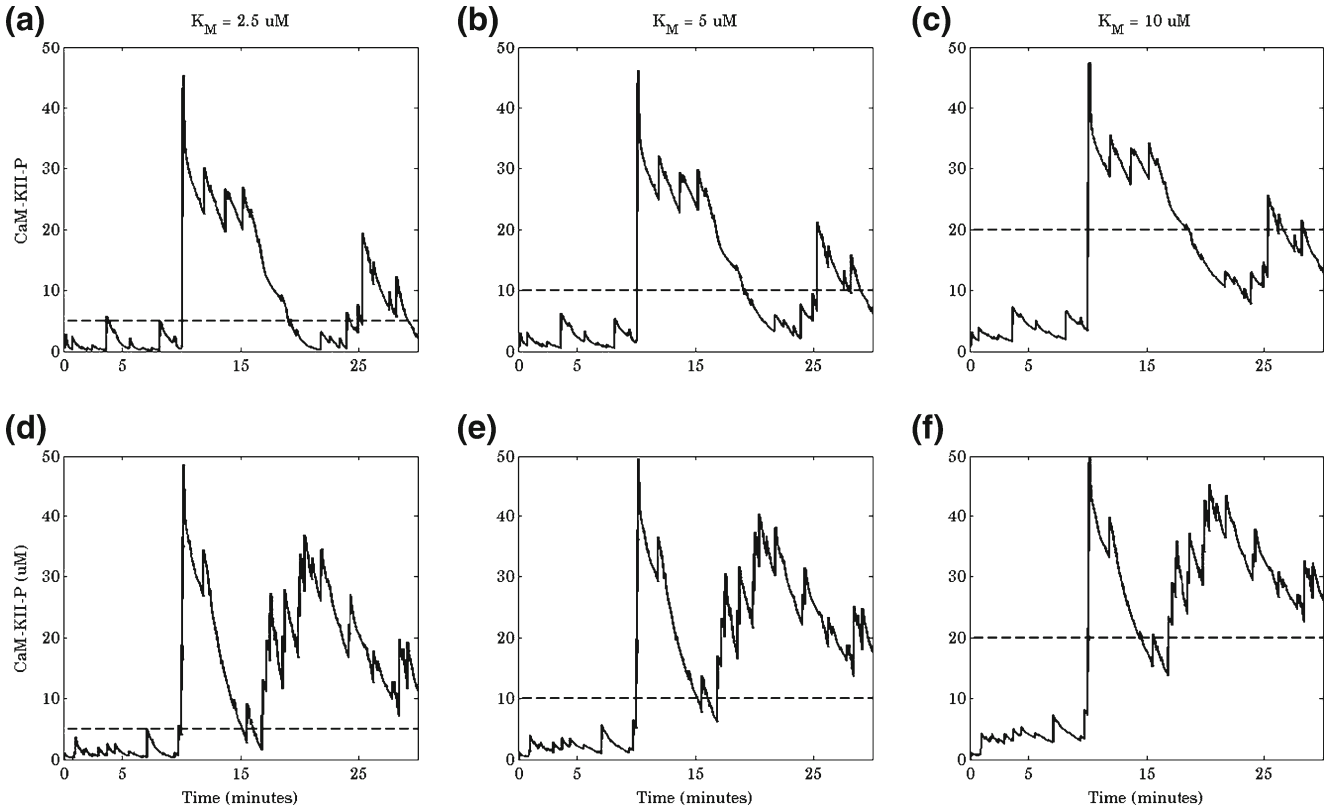

Fig. 11 Evolution of CaM-KII phosphorylation process for different values of K_M. Dotted line represents the NO production threshold set to be 5 μM, 10 μM and 20 μM for K_M values of 2.5 μM, 5 μM and 10 μM respectively. a–c are for an astrocyte-independent process. d–f are for an astrocyte-dependent process. (**a**, **d**), (**b**, **e**) and (**c**, **f**) are for K_M=2.5 μM, 5 μM and 10 μM, respectively

after ND and astrocyte stimulation: 0.35±0.04). It should be pointed out that STP observed in the experiments of Perea and Araque (2007), without post-synaptic neuron depolarization, is similar to what we observed in our simulations (experiments: from 0.24±0.03 to 0.33±0.04; simulations: from 0.26±0.04 to 0.33±0.05; before and after astrocyte stimulation). We next investigated the possible parameters which could yield us enhancement similar to what was observed in the experiments of Perea and Araque (2007), after post-synaptic neuron depolarization, in neurotransmitter release probability.

Our simulations reveal that persistent increase in neurotransmitter release probability primarily depends upon two parameters which to the best of our knowledge are not yet determined experimentally,

i) Percent increase in Ca^{2+} association rate with synaptotagmin (k_{syt}), in response to an increase in PIP_2 due to NO produced via phosphorylated CaM-KII (discussed in detail in section 2.10), and
ii) The maximal rate at which IP_3 is produced by presynaptic mGluRs (v_g).

We present and discuss results obtained, by varying these two parameters, in the following figures. We first show changes observed in the neurotransmitter release probability (Pr) when we decreased and increased the value of k_{syt}. Figure 14a and c are for k_{syt}=0.025, and Fig. 14b and d are for k_{syt}=0.1. Variation in Pr was tested under both the pathways of information processing namely, astrocyte-independent (Fig. 14a, b) and astrocyte-dependent (Fig. 14c, d).

Following suite with our earlier approach, for astrocyte-independent pathway we assumed an NP-EGTA block of astrocyte Ca^{2+} concentration and for astrocyte-dependent pathway we released NP-EGTA block of astrocyte Ca^{2+} concentration at 10 min mark (along with post-synaptic neuron depolarization). We tested if the changes in Pr prior to ND and 10 min after it are statistically significant using usual two-tailed student's test. As observed earlier in our simulations there was no statistically significant variation in neurotransmitter release probability prior to ND and 10 min after it under astrocyte-independent information processing for k_{syt} equal to 0.025 (before: 0.25±0.03; 10 min after: 0.26 ±0.04; P=0.51; see Fig. 14a) and k_{syt} equal to 0.1 (before: 0.27±0.03; 10 min after: 0.27±0.03; P=0.83; see Fig. 14b). The results are in agreement with our earlier simulations and experimental findings of Perea and Araque (2007) who found no change in Pr before and after ND when astrocyte

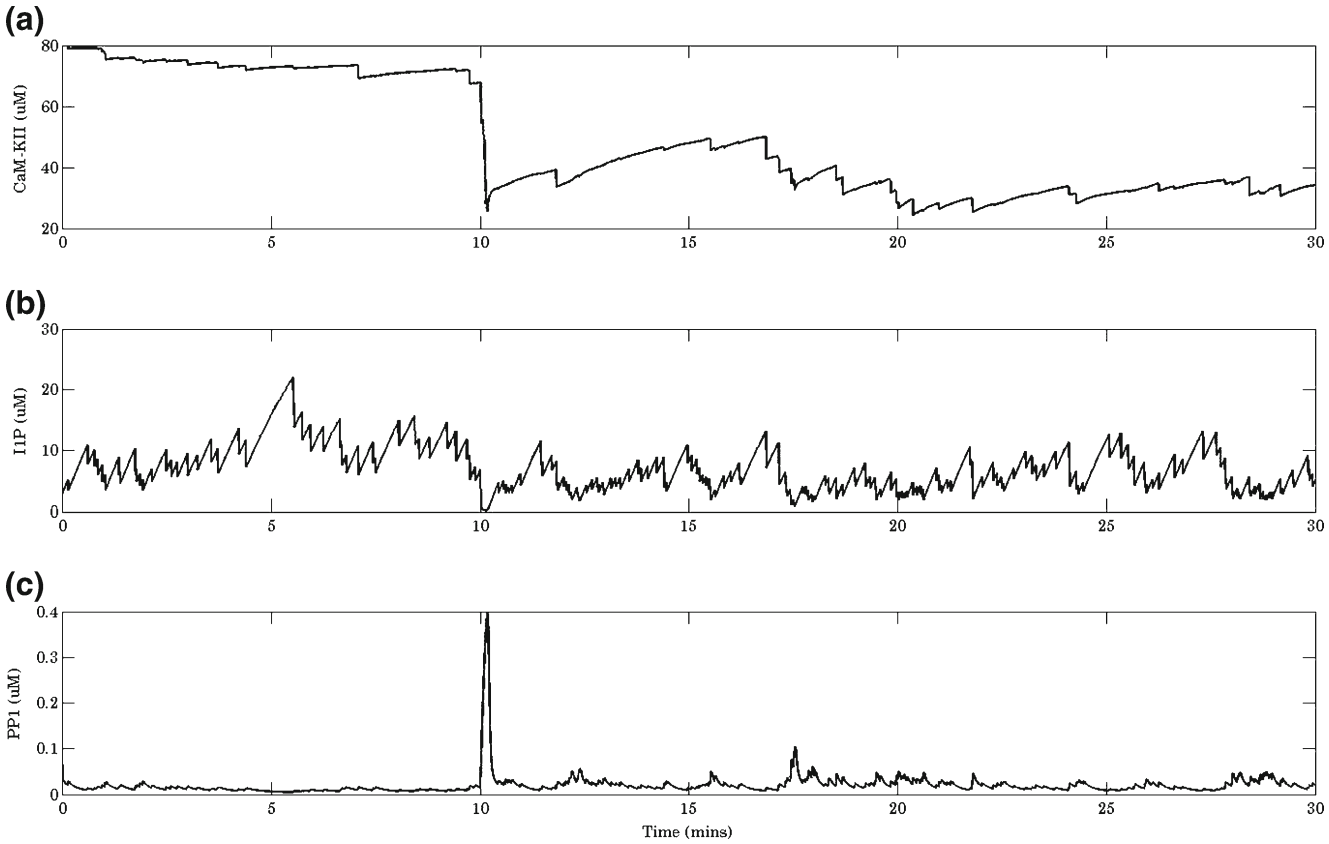

Fig. 12 Some important variables involved in CaM-KII phosphorylation process. (**a**) 0-fold phosphorylated CaM-KII, (**b**) Phosphorylated I1 (I1P), (**c**) Free PP1 i.e. not bound to I1P

was not stimulated. However we found significant change in the neurotransmitter release probability when ND was accompanied with astrocytic Ca^{2+} unblock (see Fig. 14c, d at the 10 min mark) in agreement with experiments of Perea and Araque (2007) and our earlier simulations. The changes observed in Pr before stimulus and 10 min after it were statistically significant for k_{syt} equal to 0.025 (before: 0.25 ±0.03; 10 min after: 0.35±0.04; $P<0.01$) and k_{syt} equal to 0.1 (before: 0.26±0.03; 10 min after: 0.4±0.05; $P<0.01$).

Actually varying the percent change in Ca^{2+} association rate with synaptotagmin (k_{syt}) mimics the effect of increasing PIP_2 concentration over affinity of synaptotagmin for pre-synaptic Ca^{2+} (Bai et al. 2004). For k_{syt} value of 0.025, 0.05 and 0.1 the affinity of synaptotagmin for pre-synaptic Ca^{2+} lies in intervals [9.75,10.0] μM, [9.5,10.0] μM and [9.0,10.0] μM, respectively. The value of synaptotagmin affinity is the lowest when CaM-KII is fully phosphorylated and the highest when the concentration of the phosphorylated CaM-KII is down and below the threshold for NO production ($P_{1/2}$). Being unaware of the quantitative effects of phosphorylated CaM-KII over synaptotagmin affinity we did not test the change in Pr for values of k_{syt} higher than 0.1.

We next concentrate on the other parameter namely, IP_3 production rate by pre-synaptic mGluRs, that enhances neurotransmitter release probability. The maximal rate of IP_3 production by pre-synaptic mGluR (v_g) can be expressed in terms of surface density of mGluR (ρ_{mGluR}), the surface area of bouton exposed to the extra-synaptic glutamate released by astrocyte (S), the Avogadro number N_A, the volume of bouton V_{btn}, and IP_3 molecule production rate per receptor r_p (Nadkarni and Jung 2007),

$$v_g = \frac{r_p \rho_{mGluR} S}{V_{btn} N_A}. \tag{40}$$

We could not find direct data for surface density of extra-synaptic mGluR on the bouton surface of a CA3 pyramidal cell which is an important parameter determining v_g. However, Nusser et al. (1995) determined relative densities of synaptic and extra-synaptic $GABA_A$ receptors on cerebellar granular cells using quantitative immunogold method. They estimated that synaptic $GABA_A$ receptors are 230 times more concentrated than that on the extra-synaptic membrane. Holmes (1995) suggested synaptic NMDA receptor density to be in the range of 200–2000 per μm^2. Assuming a density of 200 per μm^2 for synaptic mGluR and using relative densities of synaptic and extra-synaptic ionotropic receptors estimated by Nusser et al. (1995). We have an estimate of≈0.87 per μm^2 for surface density of

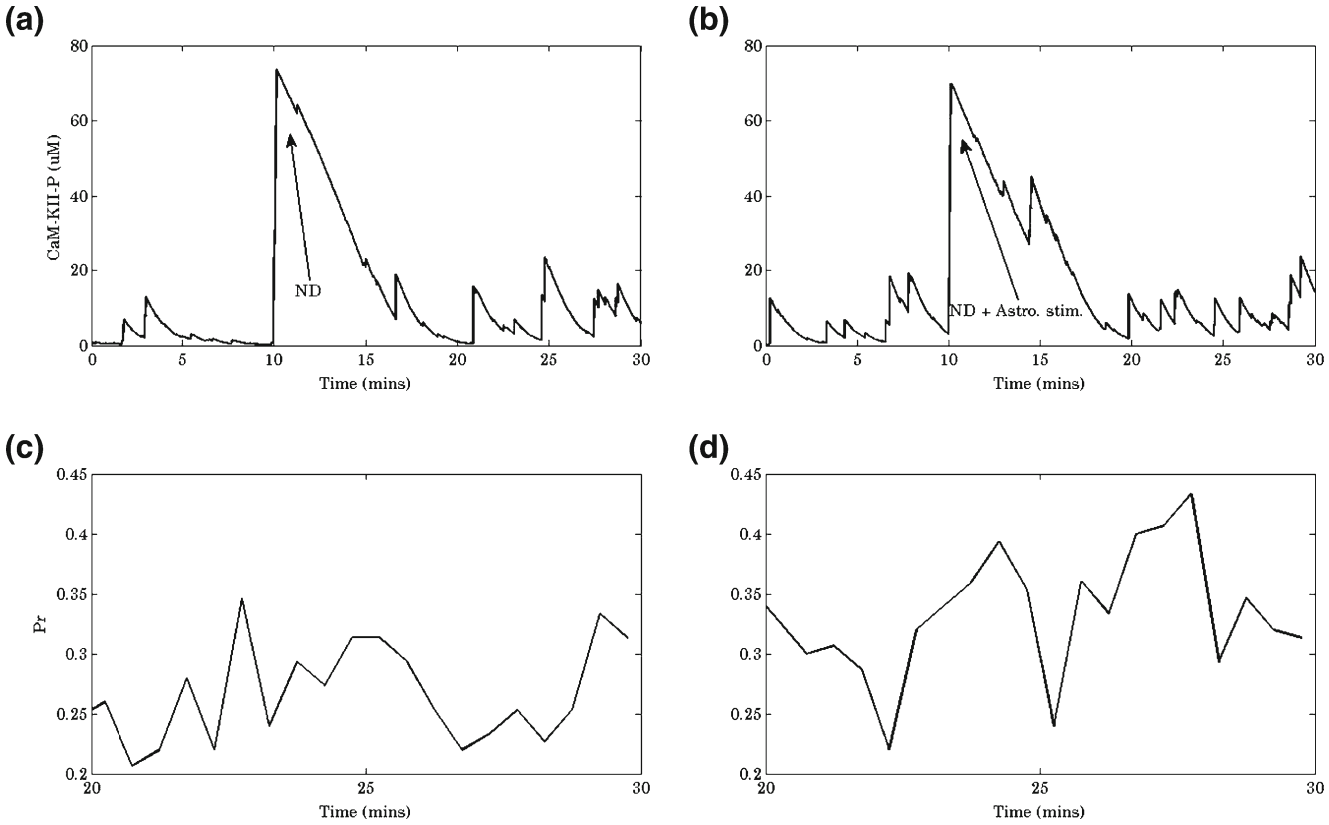

Fig. 13 The effect of post-synaptic neuron depolarization (ND) and astrocyte stimulation in absence of I1 protein. (**a**) Phosphorylated CaM-KII (CaM-KII-P) while assuming NP-EGTA block of astrocyte Ca^{2+}. (**b**) Phosphorylated CaM-KII (CaM-KII-P) when NP-EGTA block is removed at 10 min mark. (**c**) Neurotransmitter release probability (Pr) 10 min after ND, (**d**) Neurotransmitter release probability (Pr) 10 min after ND and NP-EGTA unblock. Pr was calculated as previously using a time-window of 30 s. We have shown the Fig. 13c and d from 25 min to 30 min only for the sake of clarity

extra-synaptic mGluRs on the bouton surface of the CA3 pyramidal cell.

The maximal rate of IP_3 production by mGluR on the surface of an astrocyte has been estimated to be 0.062 nM per ms (Nadkarni and Jung 2007). However, De Pittà et al. (2009) used much higher value of (0.2–0.5) nM per ms for the maximal rate of IP_3 production by mGluR on the astrocyte surface. We assumed the maximal rate of IP_3 production by extra-synaptic mGluR to be 0.062 nM per ms i.e. $\frac{0.062\times10^{-9}\times6.023\times10^{23}}{10^{-3}}$ molecules/m^3/ms or 0.373×10^{17} molecules/ms per unit volume. The average volume of a bouton at CA3–CA1 synapse is about 0.13 μm^3 (Koester and Sakmann 2000) which yields the production rate to be≈0.0048 molecules/ms. If we assume that, IP_3 molecule production per receptor is 1 molecule per ms, then the surface exposed to extra-synaptic glutamate (S) defines the maximal IP_3 production rate. For a maximal rate of IP_3 production of 0.062 (nM per ms) S is≈0.0056 μm^2. To study the effect of increasing IP_3 production rate (v_g) over Pr. We studied change in Pr for an IP_3 production rate of 0.1 nM per ms and 0.2 nM per ms. Following a similar process (which is used to determine S for v_g equal to 0.062 nM per ms) it merely implies that for an IP_3 production rate of 0.1 nM per ms and 0.2 nM per ms, 0.009 μm^2 and 0.018 μm^2 of bouton surface should be exposed to extra-synaptic glutamate released by the peri-synaptic astrocyte.

In Fig. 15, we demonstrate how astrocyte-dependent feed-forward and feed-back pathway is significantly enhanced with variation in combination of v_g and k_{syt}. The values of (v_g, k_{syt}) from Fig. 15a–d are (0.062, 0.05), (0.1, 0.05), (0.1, 0.1) and (0.2, 0.1) respectively. The purpose of the present simulations was to study the quantitative impact of these two parameters over neurotransmitter release probability after the post-synaptic neuron depolarization (ND) and astrocyte stimulation. Indeed we found and can observe a significant increase in Pr from Fig. 15a–d. We calculated Pr, as usual using a time-window of length 30 s, and tested Pr before stimulus (ND+astrocyte stimulation) and 10 min after it, for statistical significance using two-tailed student's test. Here Fig. 15a is same as Fig. 9b but is shown to demonstrate how synaptic coupling is strengthened (see Fig. 15b–d), in our model, by varying only two parameters. The neurotransmitter release probability before stimulus and 10 min after it from Fig. 15a to d increased significantly and is as follows (before: 0.25±0.03; after 10 min: 0.35±0.04; $P<$ 0.01), (before: 0.26±0.04; after 10 min: 0.41±0.06; $P<0.01$),

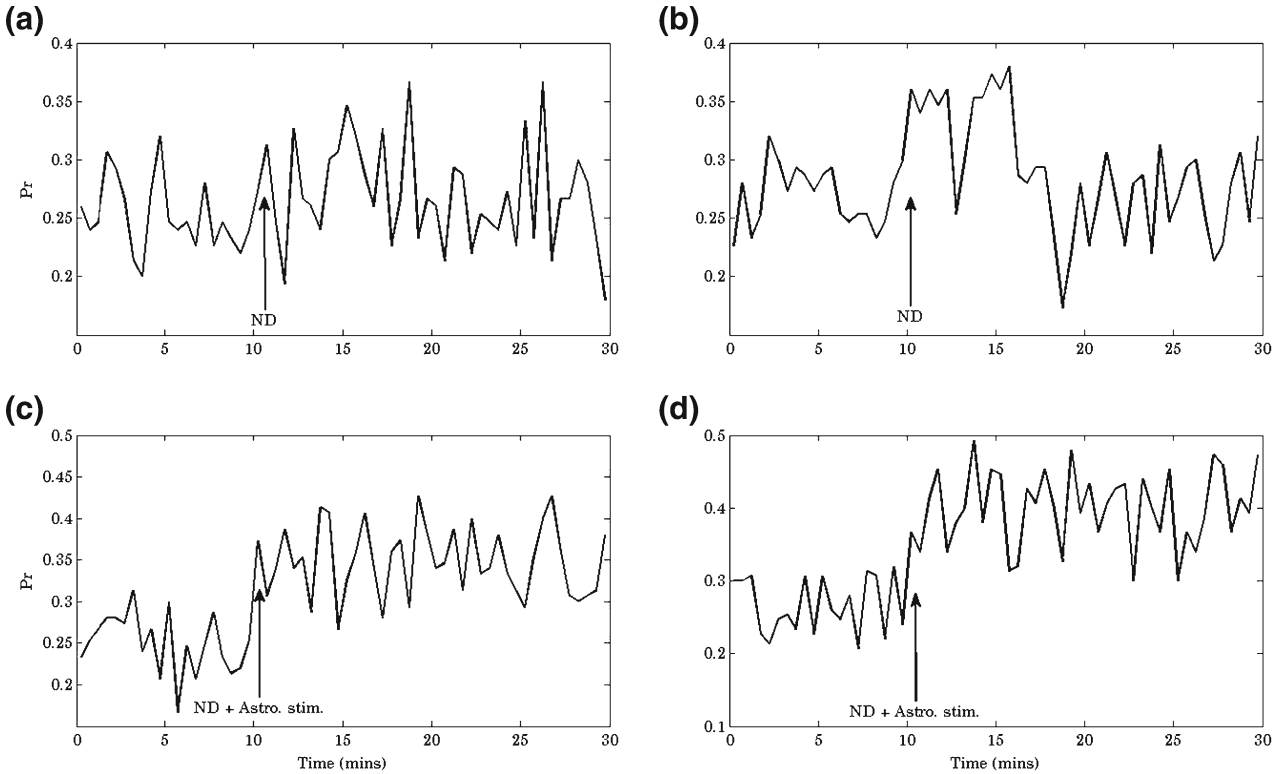

Fig. 14 Variation in neurotransmitter release probability (Pr) during astrocyte-independent (**a**, **b**) and astrocyte-dependent (**c**, **d**) pathway. All the parameters are as listed in Tables 2, 3, 4, 5, 6, 7, 8 and 9 except k_{syt}=0.025 for (**a**, **c**) and k_{syt}=0.1 for (**b**, **d**). ND, post-synaptic neuron depolarization. Pr was calculated as previously defined with a time-window of length 30 s

(before: 0.26±0.04; after 10 min: 0.48±0.06; $P<0.01$) and (before: 0.29±0.04; after 10 min: 0.57±0.07; $P<0.01$). In Fig. 15d we could observe a nearly two-fold increase in pre-stimulus to post-stimulus synaptic activities. The continuous increase in Pr observed from Fig. 15d is due to the astrocyte-dependent feed-forward (listening to the synapse) and feed-back loop (talking back to the pre-synaptic neuron). It is interesting to note that almost similar increase in neurotransmitter release probability was also observed in the experiments of Perea and Araque (2007), 10 min after pairing of ND and UV-flash astrocyte stimulation (see Fig. 4b of Perea and Araque 2007).

4 Conclusion

In this article we investigated LTP of pre-synaptic origin observed in the experiments of Perea and Araque (2007). Here we reveal a possible mechanism by which post-synaptically generated NO can regulate pre-synaptic neurotransmitter release probability. The detail underlying the proposed mechanism is currently experimentally unknown and has been modeled phenomenologically.

Since we were modeling LTP where a possible role of retrograde messenger was suspected, we included a detailed post-synaptic spine model in addition to the detailed pre-synaptic bouton and astrocyte models (see Appendix A for the important progress made in the existing model of Nadkarni et al. (2008)). We collected information about the plausible retrograde messenger likely to be responsible for the LTP observed in Perea and Araque (2007). We managed to collect evidences which point to NO as the eluding messenger (we agree that other pathways might well have been involved but NO seems more probable (Alfonso Araque, personal communication)). We eventually found a retrograde signaling pathway backed up with experimental findings see section 2.10 for details, which involves (in sequence of their involvement starting with post-synaptic spine to pre-synaptic bouton) post-synaptic calcium, CaM-KII, NO, pre-synaptic calcium, PIP_2 and synaptotagmin. We have also modeled this retrograde signaling process apart from the detailed tripartite synapse.

As we mentioned the questions to be answered were more associated with post-synaptic spine. Not much literature is available as to how exactly the pre-synaptic calcium stores are regulated by astrocytic glutamate. Therefore the classic pathways involving agonist (astrocytic glutamate) dependent IP_3 production and IP_3R mediated calcium release have been modeled. The vesicle based model proposed for glutamate release from astrocytes incorporates latest advances in glial

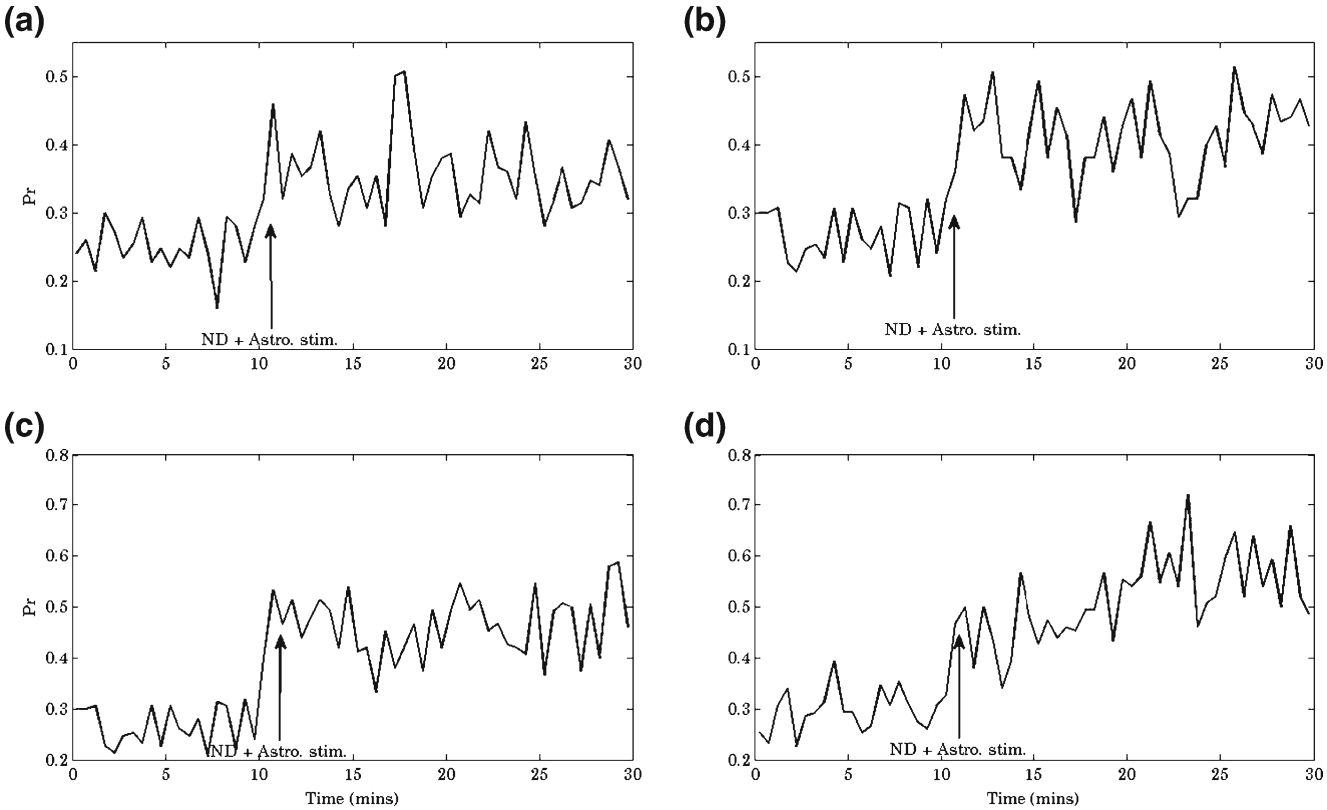

Fig. 15 Neurotransmitter release probability (Pr) enhancement using a combination maximal IP_3 production rate (v_g) and the percent increase in Ca^{2+} association rate to synaptotagmin (k_{syt}). (**a**) Is reproduction of Fig. 9b for comparison purpose, (**b**) For v_g equal to 0.1 nM per ms, (**c**) For v_g equal to 0.1 nM per ms and k_{syt} equal to 0.1, (**d**) For v_g equal to 0.2 nM per ms and k_{syt} equal to 0.1. As may be understood with the text-arrow (↑; ND+Astro. Stim.), all simulations were performed for astrocyte-dependent pathway with post-synaptic neuron depolarization (ND) and astrocyte stimulation occurring at the 10 min mark. Note that Y-axis bounds are different for (**a**, **b**) and (**c**, **d**)

pathophysiology (Malarkey and Parpura 2011) which reveal the number of releasable synaptic-like microvesicles (SLMVs) inside astrocytes and also the percentage (or probability) of SLMVs released in response to a mechanical stimulation. Both these parameters, especially the number of releasable SLMVs decides the effect of astrocyte over pre-synaptic calcium concentration and consequently on synaptic plasticity.

We tried to quantify the enhanced pre-synaptic neurotransmitter release probability observed in the experiments by Perea and Araque (2007) after the post-synaptic neuron depolarization and peri-synaptic astrocyte stimulation. Our computational study predicts two important parameters (k_{syt} and v_g) which can enhance neurotransmitter release probability and consequently synaptic efficacy at CA3–CA1 synapses. After slight modification in both the parametric values we could observe an increase in Pr (neurotransmitter release probability from pre-synaptic bouton) similar in amplitude to their experiments (simulations: from 0.29±0.04 to 0.57±0.07; experiments: from 0.28±0.04 to 0.71±0.08; before and after astrocyte stimulation). However one thing should be mentioned here that in their experiments Perea and Araque (2007) used UV-flash photolysis to stimulate astrocytes independently of the pre-synaptic neuron activity. Further the use of UV-flash could have stimulated astrocyte Ca^{2+} to an extent which might not be possible under physiological conditions (i.e. in an activity dependent manner) and hence observed a slightly higher neurotransmitter release probability in their experiments. Both these parameters are experimentally unknown at CA3–CA1 synapses. However using our modeling approach we gave an estimate for these parameters, which is in conformity with the data from the other synapses (Nusser et al. 1995; Holmes 1995; Bollmann et al. 2000).

Through computer simulations of the proposed model we demonstrate that our assumption, NO-production threshold is crossed only under astrocyte-dependent pathway, holds for under different parametric values (see Fig. 11). The validity and range of such a NO-production threshold is open for experimental testing. We also found that astrocytes help in potentiating hippocampal synapses in a feed-forward and feed-back manner, where astrocytes sense the signal transduced by the pre-synaptic neuron and feeds it back into the pre-synaptic neuron resulting in strengthening of the synapse (see Fig. 15d where such a phenomenon is clearly visible and is in close agreement with the experiments of Perea & Araque (see Fig. 4b of Perea and Araque 2007)).

Following Perea and Araque (2007) we used single pulses to stimulate pre-synaptic terminal and found that the astrocytes potentiate CA3–CA1 tripartite synapses. However we also used 0.33 Hz TBS (Epochs separated at an interval of 3 s with 1 epoch equal to 4 pulses at 100 Hz) and found an increase in synaptic efficacy (see Figure S4, provided with the electronic supplementary material) when the innervating astrocyte was turned on (but we first adjusted ρ_{Ca} so that Pr remains between 0.2–0.3 in absence of an astrocyte).

The proposed model is versatile and can exhibit STP as well, if we do not depolarize the post-synaptic neuron, similar to the experiments of Perea and Araque (2007). The model was shown to exhibit STP, in a special case, where I1 was assumed to be removed from the PSD (see Fig. 13). One more important aspect of our model is that it reaches steady-state. This mean that it continues to operate in a realistic manner with repetitive stimulations and comes to its resting conditions when not stimulated. Therefore the model is appropriate for use in situations where continued use for longer periods is necessary (e.g. LTP).

To conclude, we have formulated a realistic mathematical model of LTP (of pre-synaptic origin) at a SC–CA1 synapse modulated by an astrocyte. This model uses recent advances in astrocyte physiology which aims to classify vesicular release of glutamate from the astrocytes (Malarkey and Parpura 2011). It helped us to quantify glutamate release from the astrocyte and to improve over previously proposed models (Volman et al. 2007; Nadkarni and Jung 2007; Nadkarni et al. 2008). This model should be useful in simulating signal transduction under variety of pharmacological and pathophysiological conditions which are demonstrable in the laboratory. It will allow in-depth analysis of mechanisms behind these processes, particularly when experimental data are hard to obtain.

Acknowledgments The work has been supported by the Department of Science and Technology, Government of India, grant no. SR/CSI/08/2009. Helpful discussions and suggestions from Prof. Alfonso Araque, Instituto Cajal, Spain is being thankfully acknowledged.

Appendix A

The idea of the astrocytic feedback into the pre-synaptic terminal is not new as it has been previously modeled by Nadkarni et al. (2008). However our model is new and more challenging in the sense that it is biologically more detailed than Nadkarni et al. (2008). For example, Nadkarni et al. (2008) modeled a CA3–CA1 pyramidal cell (CA3–CA1) synapse as modulated by an astrocyte. It needs to be pointed out that the parameter values chosen by them for bouton calcium in response to an action potential (AP) are biologically not valid at the CA3–CA1 synapses. They assume that the intracellular calcium concentration rises instantly to 300 μM (and falls back to the resting values after 2 ms) in response to an AP. If we assume such high concentration then it implies that nearly $\frac{0.13\times300\times10^{-6}\times6.023\times10^{23}}{10^{15}}\approx 23490$ ions (for an average pyramidal cell bouton of volume 0.13 μm^3, Koester and Sakmann 2000) are free per AP. However the total calcium charge entering into a hippocampal pyramidal cell bouton during an AP is less than 1 fC (femto Coulomb) (Koester and Sakmann 2000). It simply implies that the total calcium ions entering a hippocampal pyramidal bouton during an AP is less than $\frac{1\times10^{-15}}{2\times1.6\times10^{-19}}-3$ 125 ions which is considerably much less than 23490 ions as discussed before. In our case, calcium entering through an AP is around 5 μM i.e. $\frac{0.13\times5\times10^{-6}\times6.023\times10^{23}}{10^{15}}\approx 392$ ions which is well under 3125 ions (maximum number of calcium ions entering into a hippocampal pyramidal bouton).

Furthermore, Weber et al. (2010) concluded that the neurons with extracellular calcium concentration of 2 mM are unlikely to have calcium sensor affinity as high as 100 μM which makes the choice of Bertram model unfavorable (since its four sensors or sites have affinities 108 nM, 400 nM, 200 μM and 1334 μM) at least for the modeling of the pre-synaptic bouton neurotransmitter release. Instead of high calcium sensor affinity Weber et al. (2010) suggested 10 μM as the best estimate for calcium sensor affinity which has been used in our model.

The astrocytic calcium dynamics used in Nadkarni et al. (2008) and in our model may seem identical in broad sense (since both of them have an agonist-dependent inositol triphosphate (IP_3) production term, agonist-independent IP_3 production term and IP_3 degradation term), but they are not. For example, the calcium-dependent term used in their model is based on the classic De Young and Keizer (1992) model which talks about phospholipase C (PLC) (which is activated by calcium) dependent IP_3 production is based on data from the experiments over the WRK1 cells (Mouillac et al. 1990), liver cells (Taylor and Exton 1987) etc. On the other hand we make use of the G-ChI model (De Pitta et al., 2009), which has a more detailed IP_3 degradation term (it incorporates inositol polyphosphate 5-phosphatase (IP-5P) and IP_3 3-kinase (IP_3-3 K) based IP_3 degradation), agonist-dependent term (it incorporates Ca^{2+}/protein kinase C (PKC)-dependent inhibitory factor over agonist-dependent IP_3 production term) and agonist-independent IP_3 production term (it incorporates PLCδ-dependent IP_3 production term) based on an astrocyte specific experiment.

References

Agulhon, C., Petravicz, J., McMullen, A. B., Sweger, E. J., Minton, S. K., Taves, S. R., Casper, K. B., Fiacco, T. A., & McCarthy, K. D.

(2008). What is the role of astrocyte calcium in neurophysiology? *Neuron, 59*, 932–946.

Agulhon, C., Fiacco, T. A., & McCarthy, K. D. (2010). Hippocampal short- and long-term plasticity are not modulated by astrocyte Ca^{2+} signaling. *Science, 327*, 1250–1254.

Anwyl, R. (2009). Metabotropic glutamate receptor-dependent long-term Potentiation. *Neuropharmacology, 56*, 735–740.

Araque, A., personal communication.

Araque, A., Parapura, V., Sanzgiri, R. P., & Haydon, P. G. (1999). Tripartite synapses: Glia, the unacknowledged partner. *Trends in Neurosciences, 22*, 208–215.

Aslam, N., Kubota, Y., Wells, D., & Shouva, H. Z. (2009). Translational switch for long-term maintenance of synaptic plasticity. *Molecular Systems Biology, 5*, 284.

Atluri, P. P., & Regehr, W. G. (1998). Delayed release of neurotransmitter from cerebellar granule cells. *The Journal of Neuroscience, 18*(20), 8214–8227.

Bai, J., Tucker, W. C., & Chapman, E. R. (2004). PIP_2 increases the speed of response of synaptotagmin and steers its membrane-penetration activity toward the plasma membrane. *Nature Structural & Molecular Biology, 11*, 36–44.

Ben Achour, S., Pont-Lezica, L., Bechade, C., & Pascual, O. (2010). Is astrocyte calcium signaling relevant for synaptic plasticity? *Neuron Glia Biology, 6*(3), 147–155.

Berridge, M. J. (2009). Module 3: Cell Signaling Biology, Portland Press Ltd. 3.1 – 3.69.

Bertram, R., Sherman, A., & Stanley, E. F. (1996). Single-domain/bound calcium hypothesis of transmitter release and facilitation. *Journal of Neurophysiology, 75*, 1919–1931.

Bezzi, P., Gundersen, V., Galbate, J. L., Seifert, G., Steinhauser, C., Pilati, E., & Volterra, A. (2004). Astrocytes contain a vesicular compartment that is competent for regulated exocytosis of glutamate. *Nature Neuroscience, 7*, 613–620.

Bibb, J. A., Nishi, A., O'Callaghan, J. P., Ule, J., Lan, M., Snyder, G. L., Horiuchi, A., Saito, T., Hisanaga, S.-I., Czernik, A. J., Nairn, A. C., & Greengard, P. (2001). Phosphorylation of protein phosphatase inhibitor-1 by Cdk5. *Journal of Biological Chemistry, 276*, 14490–14497.

Blackwell, K. T. (2005). Modeling calcium concentration and biochemical reactions. *Brains, Minds, and Media., 1*, 1–27.

Bliss, T. V. P., & Collingridge, G. L. (1993). A synaptic model of memory: Long-term potentiation in the hippocampus. *Nature, 361*, 31–39.

Bliss, T. V. P., & Lomo, T. (1973). Long-lasting potentiation of synaptic transmission in the dentate area of the anaesthetized rabbit following stimulation of the perforant path. *The Journal of Physiology, 232*(2), 331–356.

Bliss, T. V. P., Collingridge, G. L., & Morris, R. G. M. (2004). Long-term potentiation: Enhancing neuroscience for 30 years. Oxford University Press.

Bloodgood, B. L., & Sabatini, B. L. (2007). Nonlinear regulation of unitary synaptic signals by CaV2.3 voltage-sensitive calcium channels located in dendritic spines. *Neuron, 53*, 249–260.

Boehm, J., & Malinow, R. (2005). AMPA receptor phosphorylation during synaptic plasticity. *Biochemical Society Transactions, 33*(6), 1354–1356.

Bollmann, J. H., Helmchen, F., Borst, J. G. G., & Sakmann, B. (1998). Postsynaptic Ca2+ influx mediated by three different pathways during synaptic transmission at a calyx-type synapse. *The Journal of Neuroscience, 18*(24), 10409–10419.

Bollmann, J. H., Sakmann, B., & Borst, J. G. G. (2000). Calcium sensitivity of glutamate release in a calyx-type terminal. *Science, 289*, 953–957.

Bon, C. L. M., & Garthwaite, J. (2003). On the role of nitric oxide in hippocampal long-term potentiation. *The Journal of Neuroscience, 23*(5), 1941–1948.

Bradshaw, J. M., Kubota, Y., Meyer, T., Schulman, H. (2003). An ultrasensitive Ca2+/calmodulin-dependent protein kinase II-protein phosphatase 1 switch facilitates specificity in postsynaptic calcium signaling. *Proceedings of the National Academy of Sciences,* 100:10512–10517.

Calabrese, V., Mancuso, C., Calvani, M., Rizzarelli, E., Butterfield, D. A., & Stella, A. M. G. (2007). Nitric oxide in the central nervous system: Neuroprotection versus neurotoxicity. *Nature Neuroscience, 8*, 766–775.

Ching, L.-C., Kou, Y. R., Shyue, S.-K., Su, K.-H., Wei, J., Cheng, L.-C., Yu, Y.-B., Pan, C.-C., & Lee, T.-S. (2011). Molecular mechanisms of activation of endothelial nitric oxide synthase mediated by transient receptor potential vanilloid type 1. *Cardiovascular Research, 91*, 492–501.

Coffey, W. T., Kalmykov, Yu, P., & Waldron, J. T. (2005). *The langevin equation: With applications to stochastic problems in physics, chemistry and electrical engineering* (2nd ed.). Singapore: World Scientific Publishing.

Collingridge, G. L., Isaac, J. T. R., & Wang, Y. T. (2004). Receptor trafficking and synaptic plasticity. *Nature Neuroscience, 5*, 952–962.

Danbolt, N. C. (2001). Glutamate uptake. *Progress in Neurobiology, 65*, 1–105.

De Pittà, M., Goldberg, M., Volman, V., Berry, H., & Ben-Jacob, E. (2009). Glutamate regulation of calcium and IP3 oscillating and pulsating dynamics in astrocytes. *Journal of Biological Physics, 35*, 383–411.

De Young, G. W., & Keizer, J. (1992). A single-pool inositol 1,4,5-trisphosphate-receptor-based model for agonist-stimulated oscillations in Ca^{2+} concentration. *Proceedings of the National Academy of Sciences, 89*, 9895–9899.

Destexhe, A., Mainen, Z. F., & Sejnowski, T. J. (1998). Kinetic models of synaptic transmission. In C. Koch & I. Segev (Eds.), *Methods in neuronal modeling* (pp. 1–25). Cambridge: MIT Press.

Dumitriu, D., Hao, J., Hara, Y., Kaufmann, J., Janssen, W. G. M., Lou, W., Rapp, P. R., & Morrison, J. H. (2010). Selective changes in thin spine density and morphology in monkey prefrontal cortex correlate with aging-related cognitive impairment. *Journal of Neuroscience, 30*, 7507–7515.

Emptage, N. J., Reid, C. A., & Fine, A. (2001). Calcium stores in hippocampal synaptic boutons mediate short-term plasticity, store-operated Ca^{2+} entry, and spontaneous transmitter release. *Neuron, 29*, 197–208.

Erler, F., Meyer-Hermann, M., & Soff, G. (2004). A quantitative model for pre-synaptic free Ca^{2+} dynamics during different stimulation protocols. *Neurocomputing, 61*, 169–191.

Fall, C., Marland, E., Wagner, J., & Tyson, J. (2002). *Computational cell biology*. Newyork: Springer.

Fiacco, T. A., & McCarthy, K. D. (2004). Intracellular astrocyte calcium waves in situ increase the frequency of spontaneous AMPA receptor currents in CA1 pyramidal neurons. *The Journal of Neuroscience, 24*, 722–732.

Forstermann, U., & Sessa, W. C. (2011). Nitric oxide synthases: Regulation and function. Eur Heart J: ehr304.

Fox, R. F. (1997). Stochastic versions of the hodgkin-huxley equations. *Biophysical Journal, 72*, 2068–2074.

Franks, K. M., Bartol, T. M., & Sejnowski, T. J. (2002). A Monte Carlo model reveals independent signaling at central glutamatergic synapses. *Biophysical Journal, 83*, 2333–2348.

Garthwaite, J., & Boulton, C. L. (1995). Nitric oxide signaling in the central nervous system. *Annual Review of Physiology, 57*, 683–706.

Griffith, L. C. (2004). Calcium/calmodulin-dependent protein kinase II: an unforgettable kinase. *The Journal of Neuroscience, 24*(39), 8391–8393.

Hagler, D. J., Jr., & Yukiko Goda, Y. (2001). Properties of synchronous and asynchronous release during pulse train depression in cultured hippocampal neurons. *Journal of Neurophysiology, 85*(6), 2324–2334.

Helmchen, F. (2002). Raising the speed limit – fast Ca^{2+} handling in dendritic spines. *Trends in Neurosciences, 25*(9), 438–441.

Henneberger, C., Papouin, T., Oliet, S. H. R., & Rusakov, S. A. (2010). Long-term potentiation depends on release of D-serine from astrocytes. *Nature, 463*, 232–236.

Higgins, E. R., Cannell, M. B., & Sneyd, J. (2006). A buffering SERCA pump in models of calcium dynamics. *Biophysical Journal, 91*, 151–163.

Hodgkin, A. L., & Huxley, A. F. (1952). A quantitative description of membrane current and its application to conduction and excitation in nerve. *The Journal of Physiology, 117*, 500–544.

Holmes, W.R., 1995. Modeling the effect of glutamate diffusion and uptake on NMDA and non-NMDA receptor saturation. *Biophysical Journal, 69,* 1734–1747.

Hopper, R. A., & Garthwaite, J. (2006). Tonic and phasic nitric oxide signals in hippocampal long-term potentiation. *Journal of Neuroscience, 26*, 11513–11521.

Ishikawa, T., Kaneko, M., Shin, H.-P., & Takahashi, T. (2005). Pre-synaptic N-type and P/Q-type Ca^{2+} channels mediating synaptic transmission at the calyx of Held of mice. *The Journal of Physiology, 568*, 199–209.

Jafri, M. S., & Keizer, J. (1995). On the roles of Ca^{2+} diffusion, Ca^{2+} buffers, and the endoplasmic reticulum in IP_3-lnduced Ca^{2+} waves. *Biophysical Journal, 69*, 2139–2153.

Jensen, T. P., Filoteo, A. G., Knopfel, T., & Empson, R. M. (2007). Pre-synaptic plasma membrane Ca^{2+} ATPase isoform 2a regulates excitatory synaptic transmission in rat hippocampal CA3. *The Journal of Physiology, 579*, 85–99.

Kang, J., Jiang, L., Goldman, S. A., & Nedergaard, M. (1998). Astrocyte-mediated potentiation of inhibitory synaptic transmission. *Nature Neuroscience, 1*, 683–692.

Katz, B., & Miledi, R. (1970). Membrane noise produced by acetylcholine. *Nature, 226*, 962–963.

Keener, J., & Sneyd, J. (2009). *Mathematical physiology I: Cellular physiology* (Secondth ed.). New York: Springer – Verlag.

Keller, D. X., Franks, K. M., Bartol, T. M., Jr., & Sejnowski, T. J. (2008). Calmodulin activation by calcium transients in the postsynaptic density of dendritic spines. *PLoS One, 3*(4), e2045.

Koch, C. (1999). *Biophysics of computation: information processing in single neurons*. New York: Oxford University Press.

Koester, H. J., & Sakmann, B. (2000). Calcium dynamics associated with action potentials in single nerve terminals of pyramidal cells in layer 2/3 of the young rat neocortex. *Journal of Physics, 529*, 625–646.

Lee, H.-K., Takamiya, K., Han, J.-S., Man, H., Kim, C.-H., Rumbaugh, G., Yu, S., Ding, L., He, C., Petralia, R. S., Wenthold, R. J., Gallagher, M., & Huganir, R. L. (2003). Phosphorylation of the AMPA receptor GluR1 subunit is required for synaptic plasticity and retention of spatial memory. *Cell, 112*, 631–643.

Li, Y.-X., & Rinzel, J. (1994). Equations for IP_3 receptor mediated Ca^{2+} oscillations derived from a detailed kinetic model: A Hodgkin-Huxley like formulism. *Journal of Theoretical Biology, 166*, 461–473.

Lisman, J. E., & Zhabotinsky, A. M. (2001). A model of synaptic memory: A CaMKII/PP1 switch that potentiates transmission by organizing an AMPA receptor anchoring assembly. *Neuron, 31*, 191–201.

Lisman, J., Schulman, H., & Cline, H. (2002). The molecular basis of CaMKII function in synaptic and behavioural memory. *Nature Neuroscience, 3*, 175–190.

Llinas, R. (1999). *The squid giant synapse*. New York: Oxford University Press.

Malarkey, E. B., & Parpura, V. (2011). Temporal characteristics of vesicular fusion in astrocytes: examination of synaptobrevin 2-laden vesicles at single vesicle resolution. *The Journal of Physiology, 589*, 4271–4300.

Malenka, R. C., & Bear, M. F. (2004). LTP and LTD: An embarrassment of riches. *Neuron, 44*, 5–21.

Marchaland, J., Cali, C., Voglmaier, S. M., Li, H., Regazzi, R., Edwards, R. H., & Bezzi, P. (2008). Fast subplasma membrane Ca^{2+} transients control exo-endocytosis of synaptic-like microvesicles in astrocytes. *The Journal of Neuroscience, 28*, 9122–9132.

Mazzanti, M., & Haydon, P. G. (2003). Astrocytes selectively enhance N-type calcium current in hippocampal neurons. *Glia, 41*, 128–136.

McCue, H. V., Haynes, L. P., & Burgoyne, R. D. (2010). The diversity of calcium sensor proteins in the regulation of neuronal function. *Cold Spring Harbor Perspectives in Biology, 2*, a004085.

Micheva, K. D., Buchanan, J., Holz, R. W., & Smith, S. J. (2003). Retrograde regulation of synaptic vesicle endocytosis and recycling. *Nature Neuroscience, 6*, 925–932.

Miller, P., Zhabotinsky, A. M., Lisman, J. E., & Wang, X.-J. (2005). The stability of a stochastic CaMKII switch: Dependence on the number of enzyme molecules and protein turnover. *PLoS Biology, 3*(4), e107.

Montana, V., Malarkey, E. B., Verderio, C., Matteoli, M., & Parpura, V. (2006). Vesicular transmitter release from astrocytes. *Glia, 54*, 700–715.

Mouillac, B., Balestre, M. N., & Guillon, G. (1990). Positive feedback regulation of phospholipase C by vasopressin-induced calcium mobilization in WRK1 cells. *Cellular Signalling, 2*, 497–507.

Munton, R. P., Vizi, S., & Mansuy, I. M. (2004). The role of protein phosphatase-1 in the modulation of synaptic and structural plasticity. *FEBS Letters, 567*, 121–128.

Nadkarni, S., & Jung, P. (2003). Spontaneous oscillations of dressed neurons: A new mechanism for epilepsy? *Physical Review Letters 91*, 268101(4).

Nadkarni, S., & Jung, P. (2007). Modeling synaptic transmission of the tripartite synapse. *Physical Biology, 4*, 1–9.

Nadkarni, S., Jung, P., & Levine, H. (2008). Astrocytes optimize the synaptic transmission of information. *PLoS Comp. Biol., 4*(5), 1–11.

Neher, E. (1998). Vesicle pools and Ca^{2+} microdomains: New tools for understanding their roles in neurotransmitter release. *Neuron, 20*, 389–399.

Nikonenko, A. G., & Skibo, G. G. (2006). Age-related changes in synaptic vesicle pools of axo-dendritic synapses on hippocampal Ca^{2+} pyramidal neurons in mice. *Neurophysiology, 38*, 407–411.

Nikonenko, I., Boda, B., Steen, S., Knott, G., Welker, E., & Muller, D. (2008). PSD-95 promotes synaptogenesis and multiinnervated spine formation through nitric oxide signaling. *The Journal of Cell Biology, 183*, 1115–1127.

Nusser, Z., Roberts, Z. D. B., Baude, A., Richards, J. G., & Somogyi, P. (1995). Relative densities of synaptic and extrasynaptic $GABA_A$ receptors on cerebellar granule cells as determined by a quantitative immunogold method. *Journal of Neuroscience, 15*, 2948–2960.

Parpura, V., & Haydon, P. G. (2000). Physiological astrocytic calcium levels stimulate glutamate release to modulate adjacent neurons. *Proceedings of the National Academy of Sciences, 97*, 8629–8634.

Parpura, V., & Zorec, R. (2010). Gliotransmission: Exocytotic release from astrocytes. *Brain Research Reviews, 63*, 83–92.

Perea, G., & Araque, A. (2007). Astrocytes potentiate transmitter release at single hippocampal synapses. *Science, 317*, 1083–1086.

Phillips, K. G., Hardingham, N. R., & Fox, K. (2008). Postsynaptic action potentials are required for nitric-oxide-dependent long-term potentiation in CA1 neurons of adult GluR1 knock-out and wild-type mice. *The Journal of Neuroscience, 28*(52), 14031–14041.

Porter, J. T., & McCarthy, K. D. (1996). Hippocampal astrocytes in situ respond to glutamate released from synaptic terminals. *The Journal of Neuroscience, 16*(16), 5073–5081.

Rameau, G. A., Tukey, D. S., Garcin-Hosfield, E. D., Titcombe, R. F., Misra, C., Khatri, L., Getzoff, E. D., & Ziff, E. B. (2007). Biphasic coupling of neuronal nitric oxide synthase phosphorylation to the NMDA receptor regulates AMPA receptor trafficking and neuronal cell death. *The Journal of Neuroscience, 27*(13), 3445–3455.

Sabatini, B. L., & Svoboda, K. (2000). Analysis of calcium channels in single spines using optical fluctuation analysis. *Nature, 408*, 589–593.

Sabatini, B. L., Maravall, M., & Svoboda, K. (2001). Ca^{2+} signaling in dendritic spines. *Current Opinion in Neurobiology, 11*, 349–356.

Sahin, B., Shu, H., Fernandez, J., El-Armouche, A., Molkentin, J. D., Nairn, A. C., & Bibb, J. A. (2006). Phosphorylation of protein phosphatase inhibitor-1 by protein kinase C. *The Journal of Biological Chemistry, 281*(34), 24322–24335.

Schneggenburger, R., & Neher, E. (2000). Intracellular calcium dependence of transmitter release rates at a fast central synapse. *Nature, 406*, 889–893.

Schneggenburger, R., Tempia, F., & Kohnerth, A. (1993). Glutamate- and AMPA- mediated Calcium influx through Glutamate receptor channels in Medial Septal Neurons. *Neuropharmacology, 32*(11), 1221–1228.

Shuai, J.-W., & Jung, P. (2002). Stochastic properties of Ca^{2+} release of inositol 1,4,5-trisphosphate receptor clusters. *Biophysical Journal, 83*, 87–97.

Sneyd, J., & Falcke, M. (2005). Models of the inositol trisphosphate receptor. *Progress in Biophysics and Molecular Biology, 89*, 207–245.

Sochivko, D., Pereverzev, A., Smyth, N., Gissel, C., Schneider, T., & Beck, H. (2002). The CaV2.3 Ca^{2+} channel subunit contributes to R-type Ca^{2+} currents in murine hippocampal and neocortical neurones. *The Journal of Physiology, 542*, 699–710.

Taqatqeh, F., Mergia, E., Neitz, A., Eysel, U. T., Koesling, D., & Mittmann, T. (2009). More than a retrograde messenger: Nitric oxide needs two cGMP pathways to induce hippocampal long-term potentiation. *The Journal of Neuroscience, 29*(29), 9344–9350.

Taylor, S. J., & Exton, J. H. (1987). Guanine-nucleotide and hormone regulation of polyphosphoinositide phospholipase C activity of rat liver plasma membranes. Bivalent-cation and phospholipid requirements. *Biochemical Journal, 248*, 791–799.

Tsodyks, M., & Markram, H. (1997). The neural code between neocortical pyramidal neurons depends on neurotransmitter release probability. *Proceedings of the National Academy of Sciences, USA, 94*, 719–723.

Vargas, R., Cifuentes, F., & Morales, M. A. (2010). Role of presynaptic and postsynaptic IP_3-dependent intracellular calcium release in long-term potentiation in sympathetic ganglion of the rat. *Synapse, 65*(5), 441–448.

Verkhratsky, V., & Butt, V. (2007). Glial neurobiology: A textbook. John Wiley & Sons Ltd.

Volman, V., Ben-Jacob, E., & Levine, H. (2007). The astrocyte as a gatekeeper of synaptic information transfer. *Neural Computation, 19*, 303–326.

Wang, L.-Y., Fedchyshyn, M. J., & Yang, Y.-M. (2009). Action potential evoked transmitter release in central synapses: Insights from the developing calyx of Held. *Molecular Brain, 2*, 1–11.

Watanabe, Y., Song, T., Sugimoto, K., Horii, M., Araki, N., Tokumitsu, H., Tezuka, T., Yamamoto, T., & Tokuda, M. (2003). Post-synaptic density-95 promotes calcium/calmodulin-dependent protein kinase II-mediated Ser^{847} phosphorylation of neuronal nitric oxide synthase. *Biochemical Journal, 372*, 465–471.

Weber, A. M., Wong, F. K., Tufford, A. R., Schlichter, L. C., Matveev, V., & Stanley, E. F. (2010). N-type Ca^{2+} channels carry the largest current: Implications for nanodomains and transmitter release. *Nature Neuroscience, 13*, 1348–1350.

Wenker, I. (2010). An active role for astrocytes in synaptic plasticity? *Journal of Neurophysiology, 104*, 1216–1218.

Zhabotinsky, A. M. (2000). Bistability in the Ca^{2+}/Calmodulin-dependent protein kinase-phosphatase system. *Biophysical Journal, 79*, 2211–2221.